Firat Kilic BSc

Convergence of standardized RFID measurements

MASTERARBEIT

zur Erlangung des akademischen Grades

Diplom-Ingenieur

Masterstudium Elektrotechnik-Wirtschaft

eingereicht an der

Technischen Universität Graz

Betreuer

Ao. Univ.-Prof. Dipl.-Ing. Dr.techn. Erich Leitgeb

Institut für Hochfrequenztechnik

Dipl.-Ing. Jürgen Hölzl (Infineon Graz)

Graz, Juni 2015

Convergence of standardized RFID measurements

Master's Thesis

Firat Kilic

Institute of Microwave and Photonic Engineering (IHF)
Graz University of Technology
Interim Head: Univ.-Prof. Dipl.-Ing. Dr.techn. Wolfgang Bösch

supported by Infineon Technologies Austria AG

Assessor: Ao.Univ.-Prof. Dipl.-Ing. Dr.techn. Erich Leitgeb

Advisor: Dipl.-Ing. Jürgen Hölzl (Infineon Graz)

Graz, June 2015

Never stop thinking

This Master Thesis is supported by
Infineon Technologies Austria AG
Development Center Graz
Department of Chip Card and Security System
Head: Harald Witschnig

Abstract

Nowadays contactless chip cards are applied in many different fields in order to simplify our daily life. Thanks to the RFID technology contactless chip cards bring us convenience, security and efficiency. Almost every day or during our leisure time we utilize the great benefits of contactless technology for instance in contactless payment, access control systems for buildings, corporate identification cards, transport- and ticketing applications, or ePassport. Hence the contactless chip cards work impeccable for different applications they have to be tested thoroughly. During my work I learned about two important institutions, which defining specifications and testing procedures namely ISO/IEC and EMVCo. EMV test set-up is only used for payment applications and ISO/IEC 10373-6 is mainly utilized for the remaining applications. While comparing of both measuring procedures I noticed that the handling of EMV measurement is very laborious than the ISO measurement.

The main two tasks of this thesis were firstly the understanding of the main differences in measurement set-up and in measuring procedures of both test set-ups and secondly to extend the LMA-Tool in order to get EMV related values out of enhanced ISO measurements.

Keywords: RFID, Chip Card, ISO/IEC 10373-6, EMVCo, Convergence

Kurzfassung

Heutzutage werden kontaktlose Chipkarten in unterschiedlichen Bereichen eingesetzt um unseren Alltag zu vereinfachen. Dank der RFID-Technologie bringen uns kontaktlose Chipkarten Bequemlichkeit, Sicherheit und Effizienz. Beinahe jeden Tag oder auch in unserer Freizeit nutzen wir die großen Vorteile der Kontaktlosen-Technologie wie zum Beispiel bei den kontaktlosen Bezahlvorgängen, Zutrittskontrollen in Gebäuden, Firmenausweisen, Transport- und Buchungsanwendungen oder elektronischen Reisepässen. Damit die kontaktlosen Chipkarten auch einwandfrei für verschiedene Anwendungen funktionieren, müssen sie gründlich getestet werden. Während meiner Arbeit habe ich zwei wichtige Institutionen kennenglernt, welche Spezifikationen und Testverfahren definieren, nämlich ISO/IEC und EMVCo. Der EMV-Testmessaufbau wird ausschließlich für Payment-Anwendungen verwendet und ISO/IEC 10373-6 wird hauptsächlich für die restliche Anwendungen eingesetzt. Ich habe beim Vergleich der beiden Messverfahren festgestellt, dass die Handhabung der EMV-Messung aufwändiger ist als die ISO-Messung. Die zwei wesentlichen Aufgaben dieser Arbeit waren einerseits das Verstehen der Hauptunterschiede der beiden Messanordnungen im Messaufbau und im Messvorgang und in weiterer Folge das LMA-Tool zu erweitern, um EMV bezogene Werte aus der verbesserten ISO-Messung zu bekommen.

Stichwörter: RFID, Chip Karte, ISO/IEC 10373-6, EMVCo, Annäherung

EIDESSTATTLICHE ERKLÄRUNG

Ich erkläre an Eides statt, dass ich die vorliegende Arbeit selbstständig verfasst, andere als die angegebenen Quellen/Hilfsmittel nicht benutzt, und die den benutzten Quellen wörtlich und inhaltlich entnommenen Stellen als solche kenntlich gemacht habe.

Graz,am ....

(Unterschrift)

STATUTORY DECLARATION

I declare that I have authored this thesis independently, that I have not used other than the declared sources / resources, and that I have explicitly marked all material which has been quoted either literally or by content from the used sources.

....

date (signature)

Acknowledgment

I would like to express my heartfelt thanks to Infineon Technologies Austria AG for giving me the opportunity to write my master's thesis in such a friendly and helpful team. My sincerest thanks to Andrea Beit-Grogger and her successor Harald Witschnig. Next, I want to express my deep gratitude for a great support to my supervisor Jürgen Hölzl, Josef Gruber, Stephan Rampetzreiter and to all the remaining CL SYS team members. Moreover, many thanks to Professor Erich Leitgeb for being the assessor of this thesis and for his friendly support during my thesis.

My greatest thanks go to my parents Serpil and Mustafa, who have valued the importance of education. Thus they always encouraged me to study in order to find the right path for the future.

Firat Kilic

Contents

List of Figures

List of Tables

Chapter 1: Introduction and RFID Basics

The first chapter gives short general information about the *RFID system* (Radio Frequency Identification), components of the RFID systems and distinctive features of RFID systems.

During our daily life or in our leisure time we utilize the terrific advantages of the RFID systems maybe unknowingly. Nearly every day many people use contactless cards in order to enter a building or their office. In some bigger cities these systems are already used to commute to work, or as a contactless payment solution in supermarkets and modern companies track working hours by using these contactless cards. During leisure time contactless technology brings us convenience for instance at skiing, amusement parks, fitness studio or natatorium [10].
Contactless identification systems (ID systems) are called RFID systems as the power supply and the data transmission happens through magnetic fields. Contactless ID is meanwhile an interdisciplinary field which consists of radio-frequency (RF) engineering and electromagnetic compatibility, semiconductor technology, data security and cryptography, telecommunication engineering and many cognate fields.
A RFID system is congeneric with a contact-based chip card where a reader terminal supplies the chip card via its pads with energy and clock. One disadvantage of contact-based chip cards is the sensitivity of contacts for deterioration, corrosion and pollution. A contactless ID system uses also electronic data storage but the power supply of the transponder and the data communication between reader and transponder occurs over magnetic field. A pure contactless chip card has no electrical contact pads [5].

1.1 Main components of a RFID system

A RFID system consists always of at least two components namely:

Transponder: The transponder is made up of an antenna coil (also called as coupling element) in a resonant circuit and of a microchip. The chip is supplied with energy and information via the coupling system and it is able to send data from its storage. We can also say that the transponder is the data storage device of the RFID system. Transponder without an own power supply are called *passiv transponder* which means that the transponder is inactive outside of the operating volume of the reader. Within the operating volume of the reader the transponder is active and gets the required energy, clock and data from the reader [13].

Reader: Basically the reader consists of a coupling element, radio frequency module (transmitter and receiver) and a control unit. Many readers have an additional interface (RS 232, RS 485, USB...) for further processing of exchanged with the transponder. Through these interfaces data is conveyed to an other system like for instance PC's [9] [13].

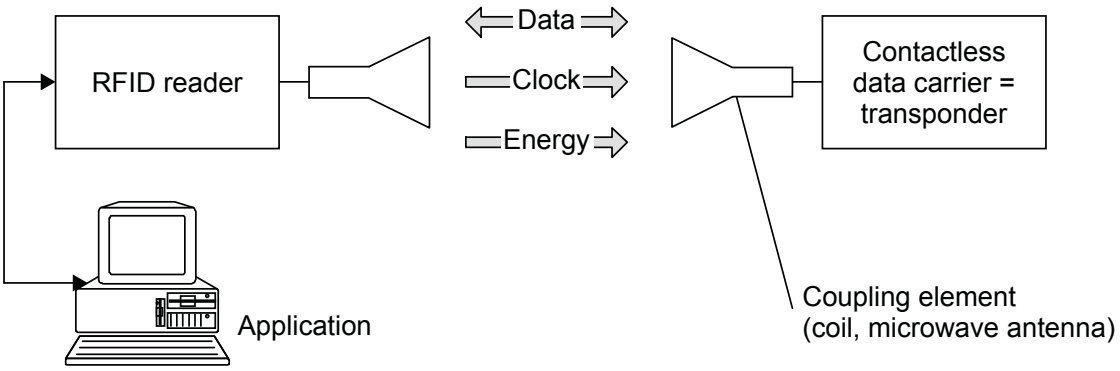

Figure 1.1: Basic structure of a RFID system [5]

1.2 Main distinctive features of a RFID system

Contactless systems are used in many different applications thus they require certain features for a respective operation in order to provide an efficient solution. The following subchapters show the main distinctive features of a RFID system [13].

1.2.1 Operating mode

Full Duplex (FDX) and Half Duplex (HDX): If the data transmisson from transponder to reader (uplink) is time-delayed to the data transmission from reader to transponder (downlink) then the mode is called half duplex. And if the transmission from transponder to reader and the transmission from reader to transponder happens simultaneously than operating mode is called full duplex. In both cases the power supply form reader to transponder is continuous and it is independent of the data transmission. The suitable transmission method for these cases is the *load modulation*, as the response of the transponder can be weak towards the signal of the reader [5] [13].

Whereas the HDX mode is the usually applied mode, the FDX mode is rarely used.

Sequential System (SEQ): The field of the reader is switched off for brief periodic phases. The transponder recognizes these intermissions and sends his response to the reader. During the intermissions the power supply fails for passiv transponders as they are supplied by the reader with energy. Implemented decoupling capacitors or backup batteries at the transponders are a remedy in order to compensate the supply gap [5] [13].

1.2.2 Power supply

The important distinctive feature is the type of the power supply of the transponder

Passive Transponder: As mentioned already in previous sections passive transponders are supplied by the field of the reader. If the transponder is not close enough to the reader then not enough energy is transmitted to the transponder and thus

the transponder is not able to start-up. As a result data can be neither transmitted nor saved by the transponder [5] [13].

Active Transponder: These special types of transponders have their own battery, which delivers the fully or partially required energy to the transponder chip. Batteries, which only supply a part of the required energy act merely as a backup battery. The received field from the reader does not serve as power supply and energy from the own power supply of the transponder through the battery does not contribute to data transmission from the transponder to the reader [5] [13].

1.2.3 Operating Frequency and Range

With the operating frequency of a RFID system is always meant the transmit frequency of the reader. In most cases,the transmission frequency of transponder and reader are equal. The different operating frequencies are assigned to three frequency bands [5] [13].

- Low Frequency (LF): 30 to 300 kHz
- High Frequency (HF): 3 to 30 MHz
- Ultra Hight Frequency (UHF): 300 MHz to 3 GHz

Additionally the RFID system can also be classified into the operating rang which derives from the operating frequency [5] [13].

- Close coupling system: 0 to 1 cm
  For safety requirements like for instance electronically door locking systems
- Proximity coupling system (ISO 14443): 0 to 10 cm
  Contactless chip cards
- Vicinity coupling system (ISO 15693): 0 to 1 m
  Smart labels and contactless chip cards
- Long range coupling: > 1 m
  UHF tags, thief protection or logistics

Chapter 2: Physical principles

It is very important and necessary to study and understand the physical interrelationships of magnetic phenomenons in order to a better and a technical understanding of the energy transportation and data transportation between reader and transponder.

2.1 Magnetic field

The basic magnetic phenomenons are described in the following subchapters.

2.1.1 Magnetic Induction B and Magnetic Field Strength H

Every current carrying conductor leads to a magnetic field which surrounds the conductor and these sourrounding magnetic flux lines are described as **H** (representing a vector) - the magnetic field strength. In contrast to electrical field lines the magnetic field lines form always closed loops [13].

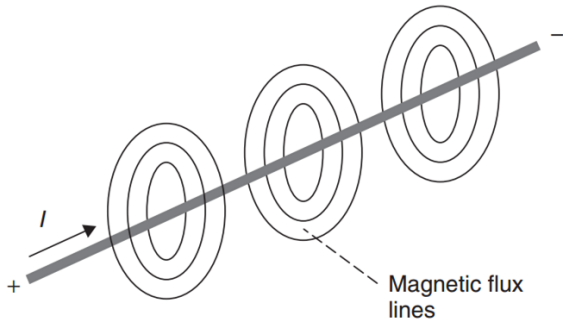

Figure 2.1: Current carrying conductor [5]

The magnetic induction **B** (representing a vector) was defined in order to consider the material properties. The following equation shows the relationship between **B** and **H**.

$$\mathbf{B} = \mu_0 \mu_r \mathbf{H} = \mu \mathbf{H} \tag{2.1.1}$$

$\mathbf{B}$	...	magnetic induction [T]
$\mathbf{H}$	...	magnetic field strength [A/m]
μ_0	...	magnetic field constant $\left(\mu_0 = 4\pi \cdot 10^{-7}\,\mathrm{Vs/Am}\right)$
μ_r	...	relative permeability of the material (e. g.: $\mu_{r,air} = 1$)

2.1.2 Ampere's law

"The relation between magnetic field strength and current is given by *Ampere's law* which states that the integration of the field strength $\mathbf{H}$ along a closed loop c equals the current, respectively the sum of currents flowing through the area spanned by the loop." [15]

Integration of the field strength $\mathbf{H}$ along only one closed loop:

$$\oint \mathbf{H} \cdot d\mathbf{l} = I \tag{2.1.2}$$

Integration over many current carrying conductors:

$$\oint_c \mathbf{H} \cdot d\mathbf{l} = \sum I_n \tag{2.1.3}$$

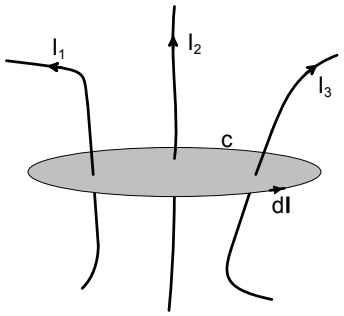

Figure 2.2: Ampere's law (adapted from [15])

Magnetomotive force:

$$\Theta = \sum I_n \tag{2.1.4}$$

2.1.3 Magnetic Flux

The magnetic flux Φ is defined as the integration of the magnetic induction $\mathbf{B}$ over an an area A [13].

$$\Phi = \int_A \mathbf{B} \cdot d\mathbf{A} \tag{2.1.5}$$

Φ corresponds the total amount of field lines of $\mathbf{B}$, which pass through an area A. Therefore $\mathbf{B}$ is also called magnetic flux density [13].

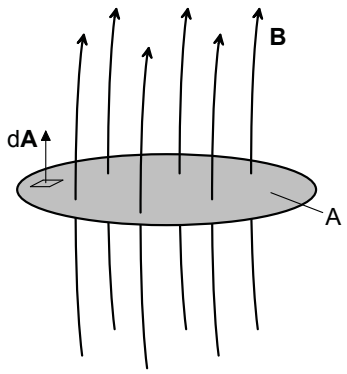

Figure 2.3: Magnetic flux (adapted from [15])

2.1.4 Lenz's law

The temporal variation of the magnetic flux Φ, which pass a loop produces in this loop an electrical current [17].

$$i \sim \frac{d\Phi(t)}{dt}. \tag{2.1.6}$$

The induced current is always aligned in such a direction so that it inhibits its cause [14].

2.2 Inductance and Mutual Inductance

The inductance serves in order to describe the magnetic coupling between the loops. A distinction is made between self inductance L and mutual inductance M [13].

2.2.1 Self Inductance

The current which flows through a loop causes a magnetic field and thereby also a magnetic flux Φ. If we put a number of loops N one above the other, which have all the same area A and through all loops flows the same current, then it results the magnetic flux linkage Ψ of all Φ of the single loops [13]:

$$\Psi = N \cdot \Phi = N \cdot B \cdot A = N \cdot \mu \cdot H \cdot A. \tag{2.2.1}$$

The self inductance L is defined as the ratio between magnetic flux linkage Ψ, which is passing through the area of a loop and the current flowing the in loop [13].

$$L = \frac{\Psi}{I} = \frac{N \cdot \Phi}{I} \qquad [H(Henry)]. \tag{2.2.2}$$

Moreover follows from law of induction:

$$u_i = \frac{d\Phi}{dt} = L \cdot \frac{di}{dt}. \tag{2.2.3}$$

The self inductance is a classifying factor for coils and it depends on the permeability(material property) of the flooded area and also on the geometry of the alignment [13].

2.2.2 Mutual Inductance

A loop 2 with an area A_2 is located near loop 1 with area A_1 and in loop 1 flows the current I_1 (assuming that both loops have only one turn N = 1). As a result of the current I_1 a part of Φ_1 will pass the area A_2. Now, both loops are coupled through the magnetic flux Ψ_{12} (coupling flux) with each other. Ψ_{12} depends on the geometry of the loops and on the permeability of the surrounding space. The mutual inductance M_{12} is defined as the ratio between Ψ_{12} and I_1 [13] [5].

$$M_{12} = \frac{d\Psi_{12}}{I_1}. \tag{2.2.4}$$

If current I_2 flow through loop 2 and thus resulting magnetic flux Ψ_{21} will pass the area A_1 of loop 1 then the following equations is valid [13] [5]:

$$M_{21} = \frac{d\Psi_{21}}{I_2}. \tag{2.2.5}$$

It applies for the the mutual inductance at consistent alignment of the loops:

$$M = M_{12} = M_{21}. \tag{2.2.6}$$

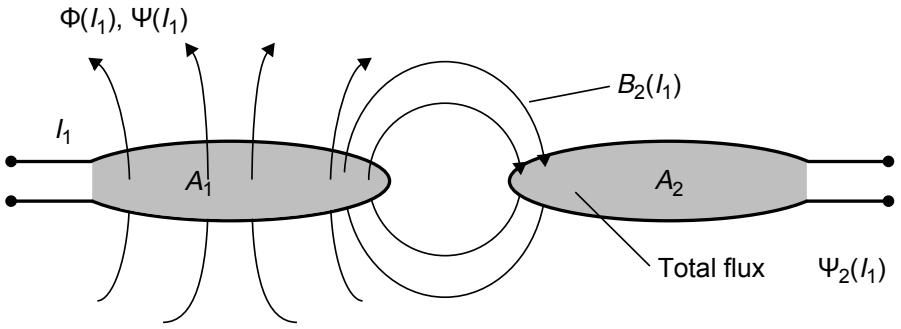

Figure 2.4: Mutual inductance (adapted from [5])

2.3 Couple Factor

The coupling coefficient k describes the coupling of two loops independent of their geometrical dimensions and it is a dimensionless quantity [13].

$$k = \frac{M}{\sqrt{L_1 \cdot L_2}} \qquad 0 \leq k \leq 1. \tag{2.3.1}$$

The value of k is between zero and one:

- k = 0: complete decoupling because of great distance between the loops or magnetic shielding
- k = 1: total coupling. This case is achieved if both loops have the same radius and if between the loops no distance exist.

2.4 Inductive Coupling

As already mentioned in previous sections, a magnetic field will always surround a current carrying conductor. The picture below shows the course of the magnetic field **H** of a loop (coil or antenna). The coil has a circular area with a radius r, which is passed by magnetic field lines.

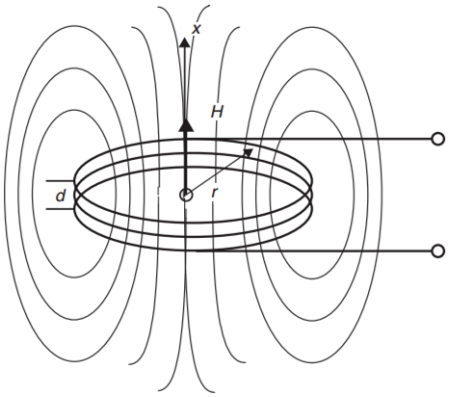

Figure 2.5: Course of magnetic flux lines of a current carrying loop (adapteded from [5])

If the magnetic field **H** is measured at different points it can be observed that **H** has the highest value in the center of circular area. It will also be noted that the value of **H** decreases if the measured point moves away along the x-axis from the center. Both core components (the transponder as well as the reader) have one own coupling element, which serves to establish the communication between each other. As coupling elements serve loops, which have the form of a cylindrical inductor and they also serve as a magnetic antenna. The coupling occurs contactless over the magnetic field which is produced by current carrying coil. Hence comes the name inductive (magnetic) coupling [13].

Figure 2.6 shows a simplified equivalent circuit of two inductive coupled coils. The coil L_1 represents the magnetic antenna of the reader and is driven by current i_1. Through i_1 a magnetic field is emitted which induces the voltage u_{i2} in the coil L_2 which again results in the current i_2. L_2 represents the magnetic antenna of the transponder. Both coils are coupled with each other through the mutual inductance M or through the couple factor k. The strength of the inductive coupling depends on the distance and position of the transponder to the reader [13].

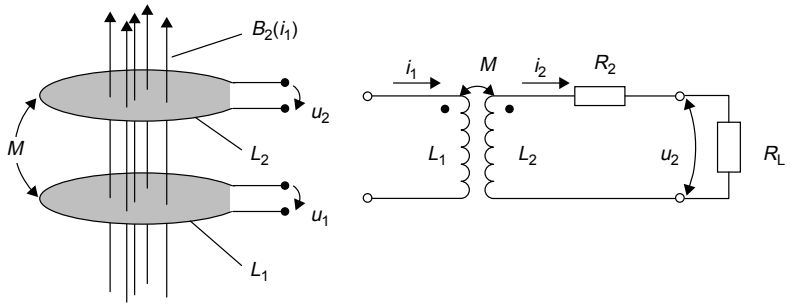

Figure 2.6: Simplified equivalent circuit of two coupled coils (adapteded from [5])

2.5 Energy Transmission

The majority of proximity cards are usually passive transponders and they get their required energy from the magnetic field of the reader. The resonance frequency of the Proximity Integrated Circuit Card (PICC) has to be accommodate to the resonance frequency of the Proximity Coupling Device (PCD) in order to increase the received energy in the PICC. The resonance frequency of the reader corresponds to 13.56 MHz and the resonance frequency of the PICC is usually adjusted between 12 MHz and 19 MHz. If both resonance frequencies are equal, then the received energy in the PICC achieves its maximum [9].

2.5.1 Series Circuit

In the following the resonance frequency of a serial circuit is deduced.

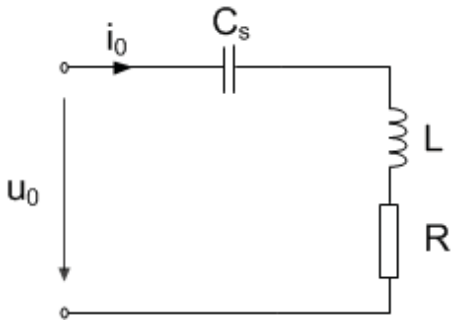

Figure 2.7: Serial circuit

The impedance $\underline{Z}_{serial}$ for series circuit:

$$\underline{Z}_{serial} = R + jwL + \frac{1}{jwC} = R + j \cdot \left(wL - \frac{1}{wC} \right) \tag{2.5.1}$$

The formula 2.5.1 shows the frequency dependence of the imaginary part and the frequency independence of the real part of the impedance $\underline{Z}_{serial}$ [16].

- $\Re\{\underline{Z}_{serial}\}$ is frequency-independent
- $\Im\{\underline{Z}_{serial}\}$ is frequency-dependent

Magnitude and phase are calculated as follows:

$$Z_{serial} = \sqrt{R^2 + \left(wL - \frac{1}{wC} \right)^2} \tag{2.5.2}$$

$$\varphi_Z = \arctan \frac{wL - \frac{1}{wC}}{R} \tag{2.5.3}$$

The current $\underline{I}$ through the circuit:

$$\underline{I} = \frac{\underline{U}}{\underline{Z}} = \frac{\underline{U}}{R + j \cdot \left(wL - \frac{1}{wC} \right)} \tag{2.5.4}$$

$$I = \frac{U}{\sqrt{R^2 + \left(wL - \frac{1}{wC} \right)^2}} \tag{2.5.5}$$

The current reaches its maximum if the $\Im\{\underline{Z}\}$ is zero. This would be the case if $w = w_0$. w_0 is called resonance angular frequency.

$$(w_0 L - \frac{1}{w_0 C}) = 0 \tag{2.5.6}$$

$$w_0 = \sqrt{\frac{1}{LC}} \tag{2.5.7}$$

$$f_0 = \frac{w_0}{2\pi} \quad resonancefrequency \tag{2.5.8}$$

$$w_0 L = \tfrac{1}{w_0 C} = \sqrt{\tfrac{L}{C}} = X_0 \quad \text{resonance reactance}$$

In case of resonance angular frequency w_0 the total impedance becomes pure real, and current $\underline{I}$ and voltage $\underline{U}$ will be in phase [16].

2.5.2 Parallel Circuit

For the derivation of the resonance frequency f_0 the admittance is considerd:

$$\underline{Y} = G + jwC + \frac{1}{jwL} = R + j \cdot \left(wC - \frac{1}{wL} \right). \tag{2.5.9}$$

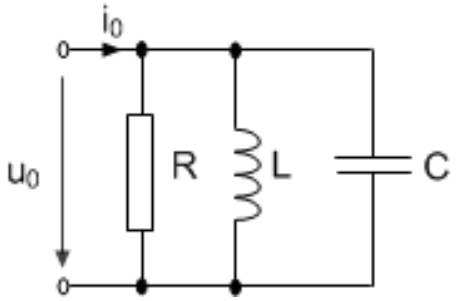

Figure 2.8: Parallel circuit

The real part of the admittance $\Re\{\underline{Y}\}$ is frequency-independent and the $\Im\{\underline{Y}\}$ is frequency-dependent. Magnitude and phase are calculated as follows:

$$Y = \sqrt{G^2 + \left(wC - \frac{1}{wL}\right)^2} \tag{2.5.10}$$

$$\varphi_Y = \arctan \frac{wC - \frac{1}{wL}}{G} \tag{2.5.11}$$

The voltage of the parallel circuit:

$$\underline{U} = \frac{\underline{I}}{\underline{Y}} = \frac{\underline{I}}{G + j \cdot \left(wC - \frac{1}{wL}\right)} \tag{2.5.12}$$

$$U = \frac{I}{\sqrt{G^2 + \left(wC - \frac{1}{wL}\right)^2}} \tag{2.5.13}$$

The voltage reaches its maximum if the $\Im\{\underline{Y}\}$ is zero. This would be the case if $w_0 = \frac{1}{\sqrt{LC}}$.

$$w_0 = \sqrt{\tfrac{1}{LC}} \quad \text{resonance angular frequency}$$

$$f_0 = \tfrac{w_0}{2\pi} \quad \text{resonance frequency}$$

$$w_0 C = \tfrac{1}{w_0 L} = \sqrt{\tfrac{C}{L}} = B_0 \quad \text{resonance susceptance}$$

2.5.3 Quality Factor

In general the quality factor Q characterizes how much the losses in a resonance circuit impact the oscillation. Q of a resonant circuit is defined over the maximum stored energy and the dissipated power [9] [16].

$$Q = \frac{w_0 \cdot \text{maximum stored energy}}{\text{dissipated power}} \mid \text{at resonance} \tag{2.5.14}$$

Q for a serial resonance circuit is described over the ratio between the reactance X_0 at resonance to the ohmic resistance R.

$$Q = \frac{w_0 \cdot L}{R} = \frac{X_0}{R} = \frac{1}{R} \cdot \sqrt{\frac{L}{C}} \tag{2.5.15}$$

The inverse of Q is called damping factor d:

$$d = \frac{1}{Q} = \frac{R}{X_0} = R \cdot \sqrt{\frac{C}{L}} \tag{2.5.16}$$

Q for a parallel resonance circuit:

$$Q_p = \frac{R_p}{X_0} = R_p \cdot \sqrt{\frac{C}{L}} \tag{2.5.17}$$

2.5.3.1 Cut-off Frequency and Bandwidth

The upper f'' and the lower f' cutoff frequencies of a resonance circuit are defined where the current I_0 (= at the resonance frequency f_0) decreases to $\frac{1}{\sqrt{2}}$ of its maximum value.

$$I = \frac{I_0}{\sqrt{2}}$$

$$\frac{1}{\sqrt{2}}\Big|_{dB} = 20 \log 2^{-\frac{1}{2}} = -10 \log 2 \approx -3dB$$

The difference of f'' - f' corresponds to the bandwidth B of resonance circuit.

$$\frac{B}{f_0} = \frac{1}{Q} \Rightarrow Q = \frac{f_0}{B}$$

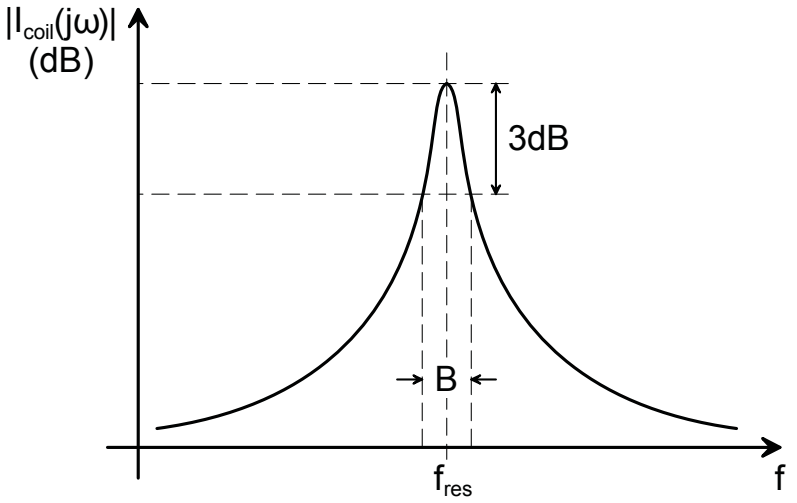

Figure 2.9: Bandwidth of a resonance circuit (adapted from [15])

With the increasing of quality factor Q decreases the bandwidth B. A high Q value leads to a better energy transfer from the reader to the transponder but simultaneously with a low B value suffers the data transmission in both directions. A compromise between Q and B has to be chosen for an efficient solution of the RFID system [9].

Chapter 3: Characterization of the system

This chapter is intended to show and explain the equivalent circuits of the PCD(reader) and the PICC(transponder). Also the the data transfer in both directions is explained in order to get a rough idea how the communication works between the core components of the contacless system

3.1 Proximity Coupling Device PCD

The Proximity Coupling Device PCD consists of the matching part which matches the antenna to the output driver of the reader which is typically 50 Ω . The matching circuit is made up of the serial capacity C_{ms} and the parallel capacity C_{mp}. The equivalent circuit of the PCD antenna is a parallel circuit. The PCD transmits continuously a high-frequency electromagnetic field through the coil L_1. The resistance R_1 represents the loss of L_1 and C_1 represents the parasitic capacitance of the antenna.
Matching circuit is necessary in order to maximize the obtained power from the source (external supply). Thus it is possible to get an antenna impedance of 50 Ω because the source also has an internal serial resistor R_i of 50 Ω. This type of matching is called power adjustment [9].

The following conditions have to be met [9]:

- $\underline{Z}_{PCD} = \Re\{\underline{Z}_{PCD}\} + j \cdot \Im\{\underline{Z}_{PCD}\}$
- $\Re\{\underline{Z}_{PCD}\} \stackrel{!}{=} 50$
- $\Im\{\underline{Z}_{PCD}\} \stackrel{!}{=} 0$

The matching capacities can be calculated in consideration of these conditions of the PCD circuit. Below the formulas for C_{ms} and C_{mp} are given [9]:

$$C_{mp} = \frac{R_i\, w\, L_1 - \sqrt{-{R_i}^2\, {R_1}^2 + R_i\, R^3 + R_i\, w^2\, {L_1}^2\, R}}{R_i\, w\, \left(R^2 + w^2\, {L_1}^2\right)} \tag{3.1.1}$$

$$C_{ms} = \frac{-{C_{mp}}^2\, w^2\, {R_1}^2 - {C_{mp}}^2\, w^4\, {L_1}^2 + 2\, C_{mp}\, w^2\, L_1 - 1}{C_{mp}\, w^2\, {R_1}^2 + C_{mp}\, w^4\, {L_1}^2 - w^2\, L_1} \tag{3.1.2}$$

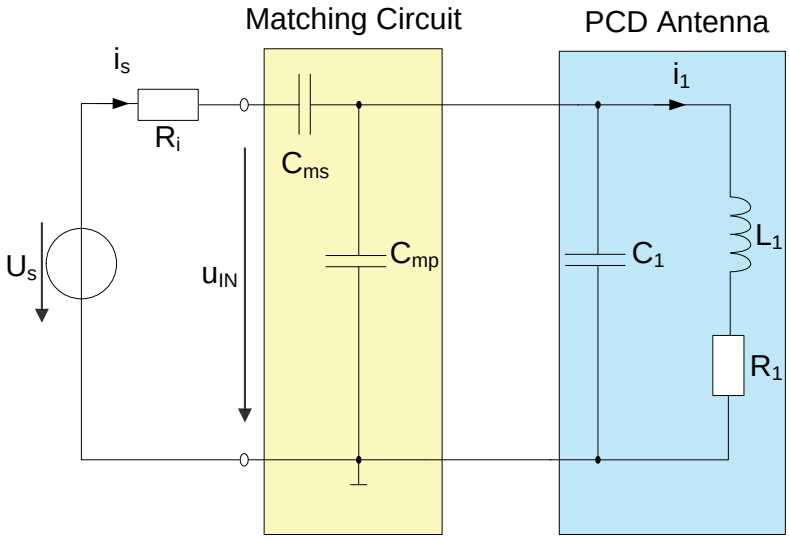

Figure 3.1: Equivalent circuit of a PCD

In general, the quality factor Q of the PCD antenna is described by the components L_1 and R_1. R_1 lowers the quality factor Q in order to ensure a certain bandwidth B for the data transfer [9].

$$Q_{coil} = \frac{w_{res} \cdot L_1}{R_1} \tag{3.1.3}$$

The quality factor Q of the whole PCD corresponds roughly [15]:

$$Q_{PCD} \cong \frac{Q_{coil}}{2} \tag{3.1.4}$$

3.2 Proximity Integrated Circuit Card (PICC)

The PICC is a passive element, which means that it does not transmit an electromagnetic field and it also does not own a battery for his own power supply. The antenna of a PICC corresponds to a parallel circuit with the coil L_2, the loss resistance of the coil R_2 and the parasitic capacitance of the antenna C_{PICC}. C_{tune} is added to the circuit in order to adjust the PICC to a specific resonance frequency for maximizing the obtained power from the PCD's magnetic field. The parallel circuit is followed up with the microchip which is represented by R_p and C_p. The whole required energy must be supplied by the PCD. PICC is the data storage device of the RFID system [9] [13].

In order to get the required power from the PCD field for the microchip the passive transponder has to be within the operating volume of the PCD. If the transponder is located within the field of the reader by means of induction an alternating voltage is induced in the PICC. The following figure shows the structure of a PICC considering the induced voltage u_{i2} [15].

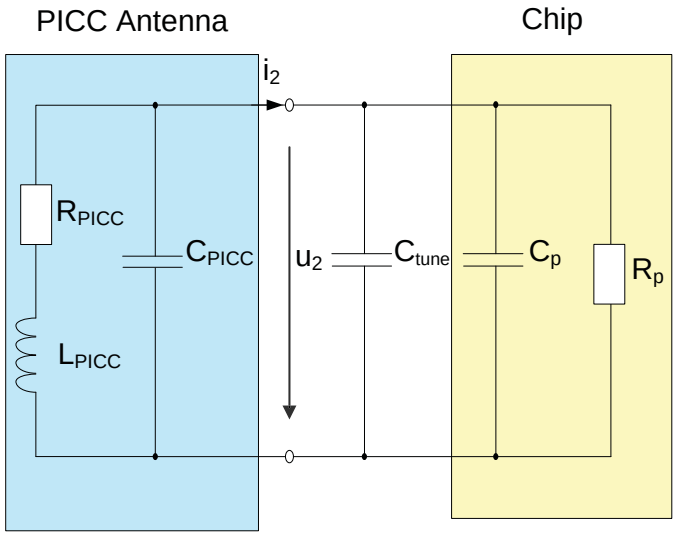

Figure 3.2: Equivalent circuit of a PICC

Voltage Regulation of the PICC:

Depending on the process technology a direct voltage between 1.2 V - 5 V is necessary for the operating voltage of the microchip in the PICC. The inductive coupling is achieved through the alternating magnetic field, thus the induced voltage in the PICC antenna as well as u_2 is an alternating voltage. Therefore u_2 must be first rectified and regulated to fit the requirements of the chip. u_2 is a measure for the induced voltage u_{i2} at the PICC antenna. Through the resonance the voltage at the transponder antenna reaches very high values. For that reason a voltage regulation in the PICC is required in order to guarantee a constant operating voltage of the data storage device. The regulation happens over a voltage-dependent shunt resistor R_s which is connected parallel to R_p. With the increasing value of u_2 the value of the shunt resistor R_s is decreasing. The quality factor of the transponder resonance circuit is always modified so that u_2 remains constant [13].

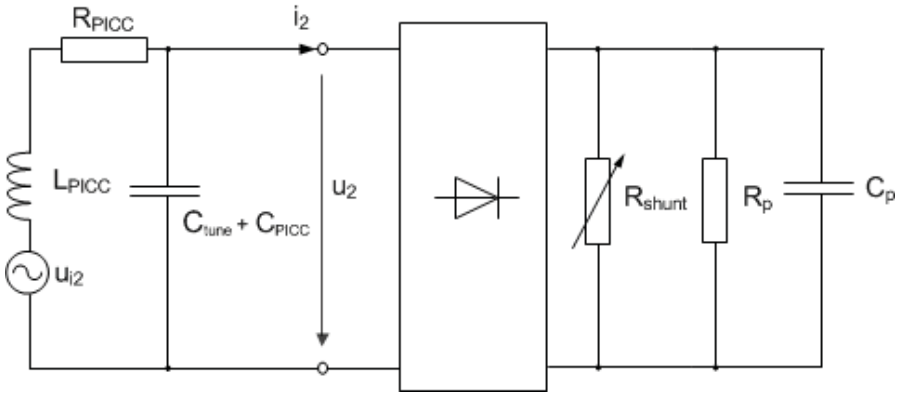

Figure 3.3: Equivalent circuit of a PICC considering rectifier and shunt resistor [15]

The figure 3.4 shows the simplified equivalent circuit of the PICC. The capacities C_{PICC}, C_{tune} and C_p are summarized as C_2. The shunt resistor R_{shunt} and R_p are combined to a load as R_L.

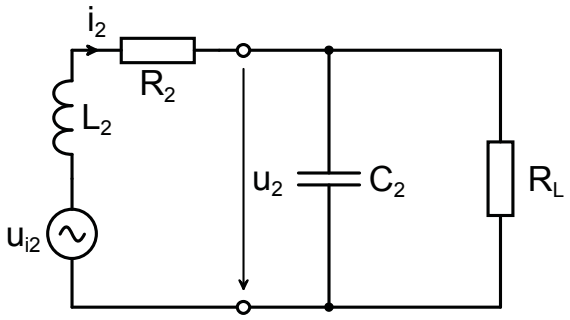

Figure 3.4: Simplified equivalent circuit of a PICC [15]

The quality factor is a measure for current and voltage increases in a resonant circuit at the resonance frequency. The following formula states the quality factor for the simplified equivalent circuit of the PICC [15].

$$Q_{PICC} = \frac{1}{R_2 \cdot \sqrt{\frac{C_2}{L_2}} + \frac{1}{R_L} \cdot \sqrt{\frac{L_2}{C_2}}} = \frac{1}{\frac{R_2}{wL_2} + \frac{wL_2}{R_L}} \tag{3.2.1}$$

3.3 Transformed Impedance $\underline{Z'}_T$

If the PICC is in the response range of the PCD then a voltage $u_{i,2}$ is induced in the antenna of the PICC (see figure 3.2). By means of the Lenz's Law (see chapter 2.1.4) i_2 counteracts over the mutual inductance M to its cause namely the current i_1 in the PCD. This leads to a variation of i_1. In general the transformed impedance $\underline{Z'}_T$ describes the feedback effect of the transponder to the antenna current i_1 of the reader. It should be noted that $\underline{Z'}_T$ is not existing as a component but it is sketched in the equivalent circuit of the PCD in order to show the feedback of the PICC. The transformed impedance $\underline{Z'}_T$ can be determined mathematically with the following formula [5] [13].

$$\underline{Z'}_T = \frac{\omega^2 k^2 L_1 L_2}{R_2 + j\omega L_2 + \frac{R_L}{1+j\omega R_L C_2}} \tag{3.3.1}$$

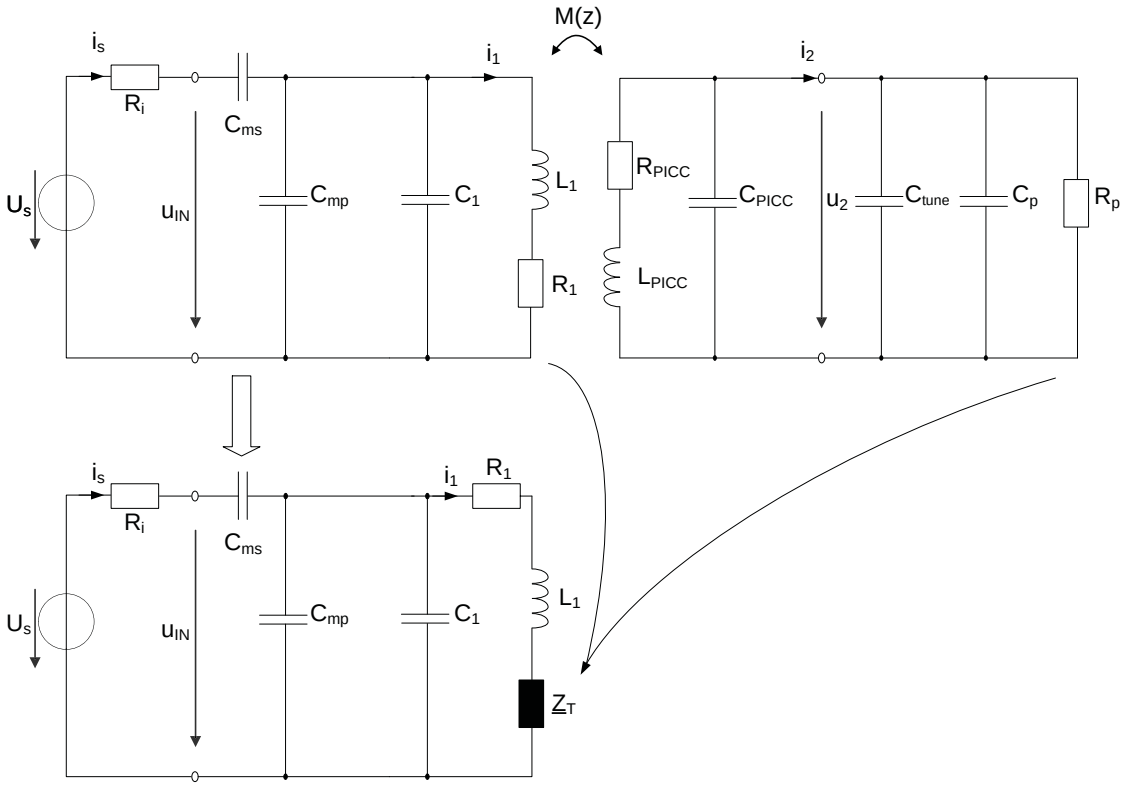

Figure 3.5: Equivalent circuit of a PCD considering feedback of a PICC [15]

$\underline{Z'}_T$ depends on various factors. The greatest influence has the coupling coefficient k [13]:

- k=0: PICC is outside of the reader's field and therefore no inductive coupling is existing $\Rightarrow \underline{Z'}_T$=0
  this case is also called *unloaded state*
- 0<k<1: If the PICC approaches to the PCD then the coupling coefficient k is increasing and thereby also the mutual inductance M. As a result also $\underline{Z'}_T$ is boosted. In case of resonance the values of $\underline{Z'}_T$ are real. Through mistuning of resonance frequency of the PICC the values of $\underline{Z'}_T$ can also contain an inductiv or a capacitiv part.
  this case is also called *loaded state*
- k=1: Only the case if both coils would have the same geometry and if both coils would lie on each other $\Rightarrow \underline{Z}_T$ reaches it maximum

3.4 Load Modulation

The modulation technique through which data are transmitted from PICC to PCD is called *load modulation*. By changing the load of the PICC according to a certain subcarrier frequency, the transformed impedance $\underline{Z'}_T$ is varied and thus the PCD current i_1. By changing the load of the PICC is actually meant that either the load resistance or the load capacitance of the transponder is varied according to the data. Due to load switching $\underline{Z'}_T$ will have understandably different values and which will influence differently the current i_1 in the reader. The result of load varying leads also to an increase or decrease of the transponder current i_2. A distinction is made between ohmic load modulation and capacitive load modulation [13] [15].

3.4.1 Ohmic Load Modulation

In the simplified equivalent circuit of the PICC a parallel resistor R_{mod} is connected to the load resistor R_L by use of a switch. If the switch is closed ,R_{mod} is connected in parallel to R_L. In this switch position the total resistance of the parallel circuit will decrease. This leads to a smaller quality factor related to (3.2.2) and a smaller value of $\underline{Z'}_T$. And if the switch is open the total resistance which corresponds to only R_L will increase and also the value of $\underline{Z'}_T$ will increase.The reader can distinguish between two values of Z_T. Ohmic load modulation corresponds rather an amplitude modulation as only magnitude is changed and the phase remain almost constant [13] [15].

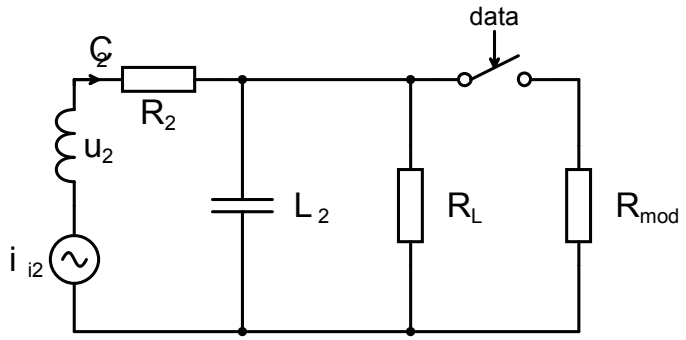

Figure 3.6: Ohmic load modulation (adapted from [15])

The formulas for $\underline{Z}_{PICC,unmod}$,$\underline{I}_{2,unmod}$ and $\underline{Z}_{T,unmod}$ in open switch position:

- $\underline{Z}_{PICC,unmod} = R_2 + j\omega L_2 + \frac{R_L}{1+j\omega R_L C_2}$
- $\underline{I}_{2,unmod} = \frac{\underline{U}_{i2}}{\underline{Z}_{PICC,unmod}}$
- $\underline{Z}_{T,unmod} = \frac{\omega^2 k^2 L_1 L_2}{R_2+j\omega L_2+\frac{R_L}{1+j\omega R_L C_2}}$

The formulas for $\underline{Z}_{PICC,mod}$,$\underline{I}_{2,mod}$ and $\underline{Z}_{T,mod}$ in closed switch position:

- $\underline{Z}_{PICC,mod} = R_2 + j\omega L_2 + \frac{R_\parallel}{1+j\omega R_\parallel C_2}, \;\; R_\parallel = \frac{R_L \cdot R_{mod}}{R_L+R_{mod}}$
- $\underline{I}_{2,mod} = \frac{\underline{U}_{i2}}{\underline{Z}_{PICC,mod}}$
- $\underline{Z}_{T,mod} = \frac{\omega^2 k^2 L_1 L_2}{R_2+j\omega L_2+\frac{R_\parallel}{1+j\omega R_\parallel C_2}}$

3.4.2 Capacitive Load Modulation

If a parallel capacitance C_{mod} is added instead of R_{mod} then the parallel circuit consists of C_2, R_L and C_{mod}. In the closed switch position the value of the total parallel capacitance will increase that will lead to a detuning of the resonance frequency of the transponder and this switch position will result in a variation of magnitude and phase of Z_T. Therefore can be said that capacitive load modulation is a mix of amplitude and phase modulation (ASK,PSK) [13] [15].

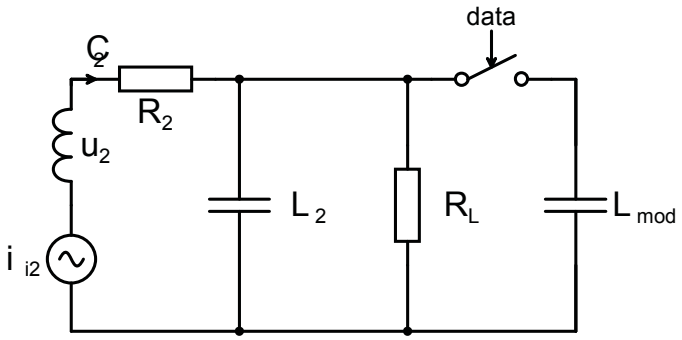

Figure 3.7: Capacitive load modulation (adapted from [15])

Chapter 4: ISO/IEC 14443 and EMVCo

This chapter tries to give main information regarding structure and measuring procedures of both test set-ups which were especially helpful and relevant for understanding of the main task.

4.1 ISO Test Set-up

ISO and IEC are the abbreviations for *International Organization for Standardization* and *International Electrotechnical Commission*. The functionality and operating parameters of *contactless* proximity coupling chip cards are described in detail in ISO/IEC 14443. The various test procedures of contactless chip cards are explained in ISO/IEC 10373 Part-6 [12].

4.1.1 ISO/IEC 14443 - Proximity integrated circuit(s) cards

ISO/IEC 14443 consists of four parts:

- Part 1: Physical characteristics
- Part 2: Radio frequency power and signal interface
- Part 3: Initialization and anticollision
- Part 4: Transmission protocols

In the following only the main points of Part 2 are briefly described. This is as particularly important and helpful for understanding of the main assignment. For further and detailed information see [11].

Part 2 - Radio frequency interface:

The PICC gets the needed power supply via the alternating magnetic field of the PCD, which uses a transmission frequency f_t of 13.56 MHz. The card contains a coil with usually 3 to 6 turns.
The generated magnetic field of the PCD has to be within 1.5 A/m $\leq H \leq$ 7.5 A/m for ID-1 cards. Hence the minimum operating field strength H_{Min} of a PICC is 1.5 A/m $\leq H_{Min}$.The minimal field strength H_{Min} means that at this value the chip of the transponder has barely enough voltage supply for operating.
There are two different methods of data transmission between PCD and PICC, namely type A and type B. The chip card needs only to support one of the two transmission techniques, while the reader has to support both techniques in order to communicate with all type of cards. Polling is used during the idle time in order to switch between the two transmission techniques. But during an existing communication between reader and transponder it is not allowed to switch between these two transmission types [5].

Communication from PCD to PICC:

	Type A	Type B
Modulation	100% ASK with modified Miller-coding	10% ASK with NRZ-coding

Table 4.1: Communication from PCD to PICC [5]

Communication from PICC to PCD:

	Type A	Type B
Modulation	Load Modulation with subcarrier $f_{sub} = 847kHz$ (13.56 MHz/16)	Load Modulation with subcarrier $f_{sub} = 847kHz$ (13.56 MHz/16)
Subcarrier Modulation	ON-/OFF-keying with Manchester-coding	BPSK with NRZ-coding

Table 4.2: Communication from PICC to PCD [5]

The proximity coupling system operates with four different bit rates according to the ISO/IEC standard 14443. In the tables 4.1 and 4.2 the bit rate 106 kBit/s (13.56 MHz/128) is shown with the according subcarrier modulations and coding procedures. For detailed information about the remaining communication interfaces see [11].

4.1.2 ISO/IEC 10373 Part-6

ISO/IEC 10373 Part-6 describes in detail the dimensions of the main components of the test set-up and the test procedures of relevant parameters like for instance the operating field strength range (H_{Min} and H_{Max}) or the voltage load modulation amplitude (VLMA). In general the structure of the test method consists of:

- Calibration coil
- Test PCD assembly
- Reference PICC

In the following the measuring with the test set-up is described. Furthermore, brief information about VLMA is given because within this thesis only a simple field strength sweep measurement of a chip was sufficient. No further special measurements or calculations were done.

4.1.3 VLMA

The VLMA can be determined with the ISO test set-up (figure 4.2). The amount of the VLMA serves as quality criterion of load modulation in PICC. The *Discrete Fourier Transformation* of at least six cycles of the waveform of the subcarrier load modulation (corresponds also to the modulated current i_2) is calculated in order to get the VLMA values. The transformation delivers the modulated signal in the frequency domain. The amplitudes at the frequencies $f_t - f_m$ (lower side band) and $f_t + f_m$ (upper side band) correspond to the LMA values. For further and accurate information about VLMA see recommendation [11].
The ISO/IEC 14443 also defines the limits for the minimal VLMA values, which are depending on the adjusted field strength. As already mentioned before, the operating

field strength for ID-1 cards has to be between 1.5 A/m $\leq H \leq$ 7.5 A/m. The following formulas specify the minimal VLMA values of PICC and PCD for Class 1 PICC.

$$V_{LMA,PICC} = \frac{22}{\sqrt{H}} \tag{4.1.1}$$

$$V_{LMA,PCD} = \frac{18}{\sqrt{H}} \tag{4.1.2}$$

$V_{LMA,PCD}$ describes the minimum VLMA value which has to be correctly detected by the PCD. In the following figure the curves for minimum VLMA are depicted dependent on the operating field strength [11].

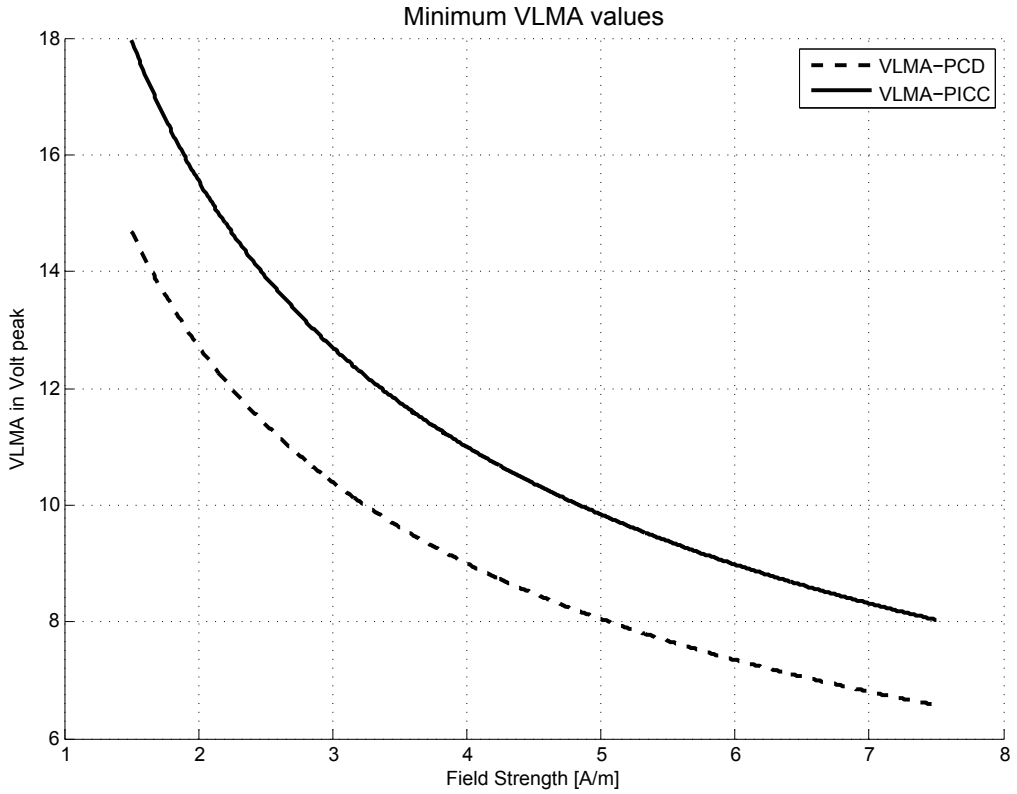

Figure 4.1: Minimum VLMA values according to ISO/IEC 14443 [11]

4.1.4 Test assembly

The ISO test set-up for proximity cards (figure 4.2) consists of two parallel sense coils and one PCD antenna which is driven by an alternating current. Thus PCD is generating the magnetic field and it is located between the two sense coils. Through this constitution the test set-up is also called ISO-tower. Both sense coils are connected in phase opposition to each other so that the induced voltages in both sense coils cancel each other at unloaded state. Additionally both sense coils have the same distance to the PCD. The sense coil A (above the PCD) and the the sense coil B (below the PCD) form a measuring bridge.
The device under test DUT (PICC) is placed on the center of the sense coil A and the calibration coil which serves to measure the field strength is mounted at the bottom of the sense coil B.
While measuring the induced voltages in the coils a high impedance oscilloscope probe ($C_p < 14pF$) shall be used [12]. Thanks to the ISO-tower, the differential voltage u_d between the sense coils is proportional to the current i_2. The couple factor between PCD and PICC $k_{PCD,PICC}$ and the couple factor between PCD and the calibration coil $k_{PCD,CAL}$ are equal as the both have the layout (ID-1 card) and the same distance to PCD coil [9].
To sum up the ISO-tower, it can be said that, PCD antenna is supplied by an *Arbitrary Waveform Generator* AWG whereby the magnetic field is induced and in order to analyze a contactless chip card the ISO-tower has two measuring points. With a digital sampling oscilloscope the voltage at the calibration coil and the differential voltage u_d of sense coils are measured. This serves for further and accurate analysis.
For a detailed description see the recommendation [9].

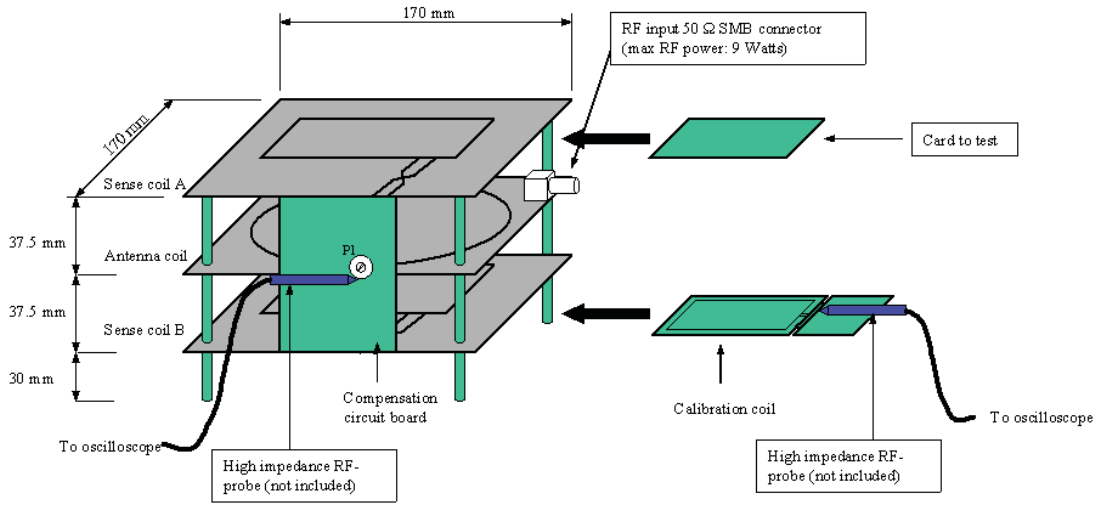

Figure 4.2: ISO-Measurement set-up (adapted from [9])

4.2 EMVCo

EMV stands for *Europay, MasterCard and Visa*. The global EMV Integrated Circuit Card Specifications for Payment Systems were first published in 1996 and are administered by the EMVCo. These specifications were defined in order to enable a successful payment between chip based consumer payment applications and acceptance terminals. The EMV chip cards are applied in credit and debit payment. In general the secure chip is embedded in a plastic payment card and it offers the following key properties [3] [6]:

- it can save information
- it can execute processing
- it is able to save secret information securely and
  also execute cryptographic processing

The chip card based payment might be contact-based, contactless or both contact-based and contactless. Chip cards which support both interfaces are also called dual interface. For contact-based applications the chip must be in galvanic contact with the reader and for a successful contactless payment transaction the chip has to be located in a certain distance to the reader (a maximum of 4 cm) [3].

4.2.1 EMV Contactless Level 1 Test Equipment

The EMV Contactless Level 1 Test Equipment consists of:

- EMV-Test PCD
- Operating Volume
- EMV-Test PICC
- EMV-Test CMR (Common Mode Rejection)

4.2.1.1 EMV-Test PCD

The figure 4.3 shows the EMV-Test PCD which consists of a printed circuit board PCB and a stand made of perspex. The PCD consists of an antenna and a corresponding matching circuit, which is connected via the J1 SMA socket with an amplifier and an *Arbitrary Waveform Generator* AWG. Thus commands can be sent via PCD antenna to the PICC. Additionally, the input impedance at J1 at unloaded state (no PICC within the PCD field) corresponds 50 Ω at 13.56 MHz (see figure 4.4). J2 delivers the voltage drop U_{Rs} over the shunt resistance R_s, which has the value of 1 Ω. In contrast to ISO test assembly, the EMV-Test PCD determines the response of the PICC through U_{Rs}, which also corresponds to the current of PCD antenna.

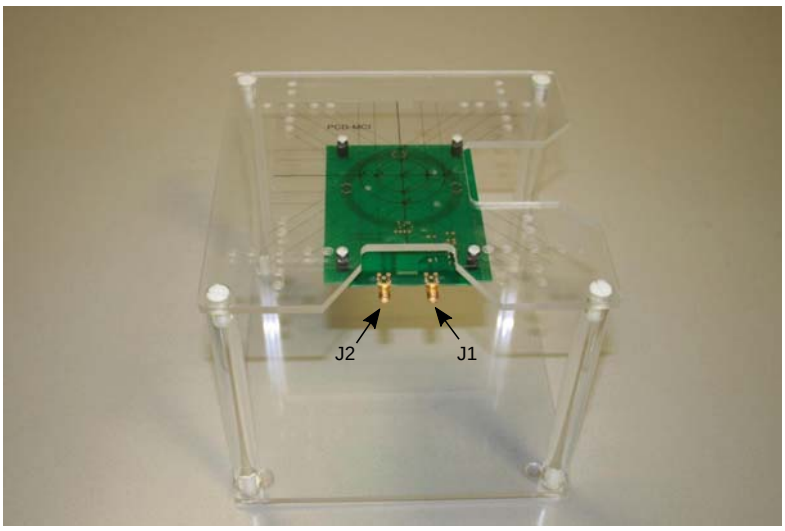

Figure 4.3: EMV PCD (adapted from [4])

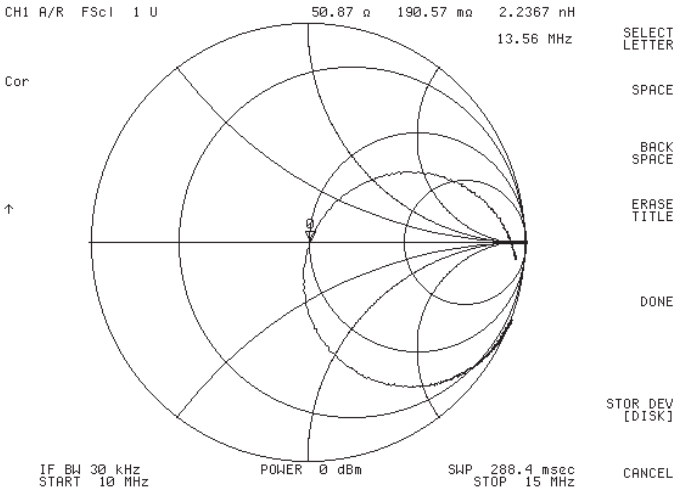

Figure 4.4: Measurement at J1: PCD Unloaded-state at 13.56 MHz

4.2.1.2 Operating Volume

The operating volume made of perspex (figure 4.5) is located on the top face of the stand and it can be shifted to certain positions on this plane. Thus all valid testing measurement positions between PCD and PICC are given and where they can communicate impeccably with each other. The figure 4.6 shows the various positioning options on the top face of the PCD. The different position options of a PICC within the operating volume are given by the triplet (z,r,φ). The operating volume is located in the center position if r=0, which also simultaneously means φ=0. The inner circle corresponds to r=1 and the outer circle corresponds to r=2. The following table shows the values for φ in different coordinates [2]:

Value of Coordinate	Value of Label Points
$\varphi = 0$	φ=0
$\varphi = \pi/2$	φ=3
$\varphi = \pi$	φ=6
$\varphi = 3\pi/2$	φ=9

Table 4.3: Label point identifiers and associated ϕ value [2]

The operating volume has five slots in which a PICC can be placed, hence the distance between PCD and PICC is represented by the value of z.

- Slot 0 $\Rightarrow$ z=0
- Slot 1 $\Rightarrow$ z=1
- Slot 2 $\Rightarrow$ z=2
- Slot 3 $\Rightarrow$ z=3
- Slot 4 $\Rightarrow$ z=4

With the increasing slot number the PICC moves away from the PCD, thus the impact of PICC to PCD is decreasing. As already explained, the impact of PICC to PCD is described by $\underline{Z}'_T$. The coupling coefficient k indicates how well the coils are coupled with each other and it decreases with increasing slot number.
The investigation of this thesis was limited to the following positions (z,0,0). That means, the operating volume is located in the center and the PICC is varied only in z-axis by positioning it in different slots.

Figure 4.5: Operating Volume (adapted from [1])

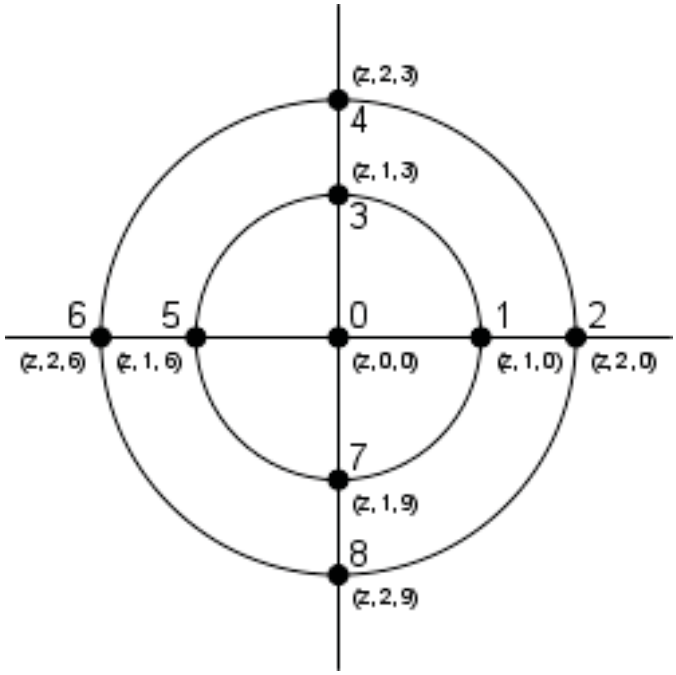

Figure 4.6: EMVCo Orientation (adapted from [2])

4.2.1.3 EMV-Test PICC

As a result of a compromise between power consumption, detuning, and communication capability the resonance frequency f_{Res} of the EMV-Test PICC is tuned to 16.1 MHz. Furthermore, it serves various functions [2]:

- Field strength measurement of the PCD (at J1)
- Sending PICC emulated data to the PCD being tested (at J2)
- Sensing of the PCD signal via the PICC pickup coil (at J9)

Jumper J7 adjusts the EMV-Test PICC load and jumper J8 sets the EMV-Test PICC load type. The socket J3 is not used. Within this thesis only the J1 connection is used in order to set up the nominal power of the EMV-Test PCD. For more information about each component of the EMV-Test PICC see [2].

How to set up the nominal power of the EMV-Test PCD?

The following four steps describe the nominal power adjustment [2]:

Step	Action
Step 1	The EMV-Test PICC is located in position (z=2, r=0, φ=0) of the operating volume of the EMV-Test PCD. Additionally, the default settings of the jumpers have to be adjusted: J7: 1 - 3 and J8: 1 - 4
Step 2	J1 of the EMV-Test PICC is connected with the oscilloscope with which an average voltage is measured
Step 3	The signal generator is regulated until the nominal power of 5.53V is measured at J1 of the EMV-Test PICC
Step 4	Remove the EMV-Test PICC from operating volume and do not change the voltage adjustment of the signal generator

Table 4.4: Nominal power adjustment of the EMV-Test PCD [2]

Step 4 of the nominal power adjustment indicates the main difference between the EMV measurement and the ISO measurement, namely that the field strength remains constant and only the position of the PICC varies. For the ISO measurement the DUT has a fixed position and the field strength varies.

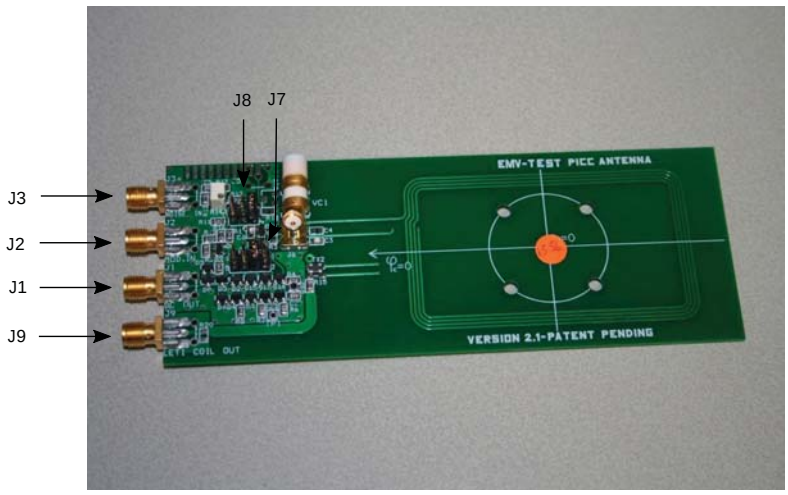

Figure 4.7: EMV PICC (adapted from [4])

4.2.1.4 EMV-Test CMR

"The aim of the EMV - TEST CMR is to form a signal switching and conditioning unit for the test bench. It is expected that it would be connected to J2 of the EMV - TEST PCD, J9 of the EMV - TEST PICC and the analogue to digital converter of the test bench." [4]
For the sake of completeness the EMV-Test CMR is also mentioned but it was not used within this thesis.

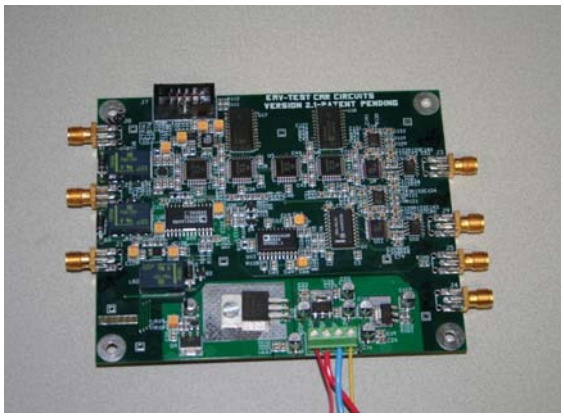

Figure 4.8: EMV CMR (adapted from [4])

4.2.2 Simplified equivalent circuit of EMVCo set-up

This subsection describes the electrical equivalent circuit in more detail which is also implemented in LMA-Tool and it was also used for simulation in *Advanced Design System* (ADS). It is also showed how the parameters of the equivalent circuit are determined through measuring and calculation. The following simplified figure should result in a better understanding of the EMVCo set-up. As previous mentioned, the field strength remains constant (through nominal power adjustment) and only the position of the PICC is varied through the operating volume. The variation of PICC position leads to a different mutual inductance $M(z)$ between PCD and PICC. The simplified electrical equivalent circuit is depicted in figure 4.10.

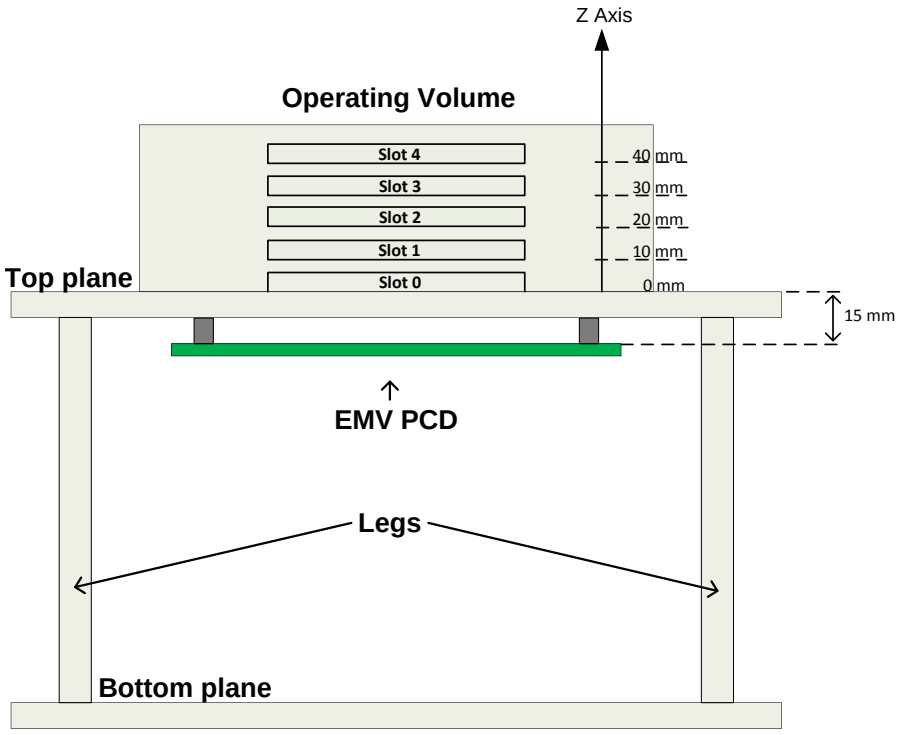

Figure 4.9: Front view of the EMVCo set-up

The focus of this thesis is to measure the **Loading Effect** (RX-mode) and the **LMA** (TX-mode) at the positions **(z,0,0)** and to compare them with the LMA-Tool results.

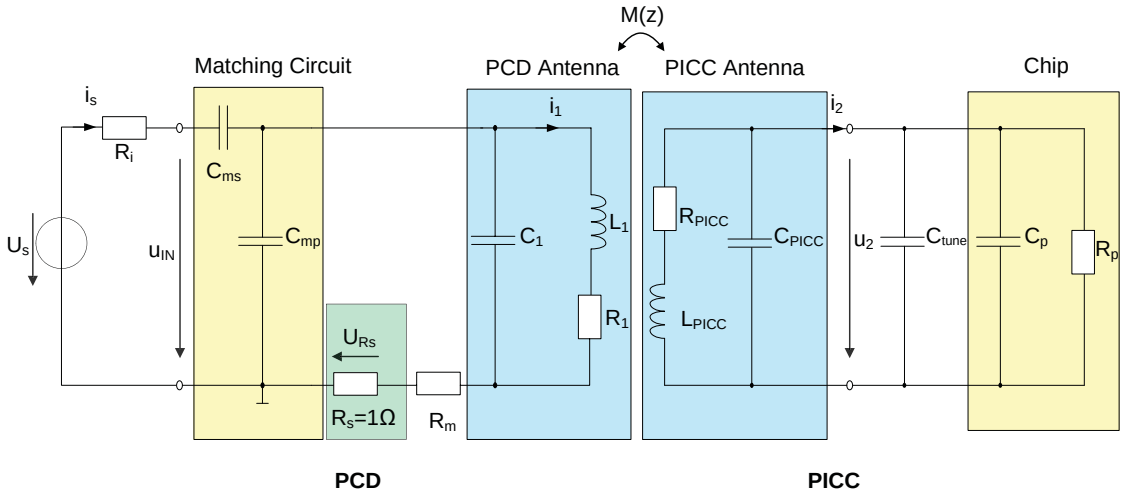

Figure 4.10: Simplified electrical equivalent circuit

The voltage source of the PCD is driven by a frequency of 13.56 MHz and its internal resistance R_i corresponds to 50 Ω. The matching circuit, which consists of the serial capacity C_{ms} and the parallel capacity C_{mp} is necessary for an efficient use of the power of the voltage source. It matches the PCD antenna to R_i of the voltage source.
EMVCo set-up investigates the current through the shunt resistance R_s which is modulated through the impact of the PICC. It does not examine any of the PICC parameters. This current simultaneously corresponds to the voltage drop U_{Rs}. It is determined by the amplitude difference of the states (like, for instance, Loading = $U_{Rs,unloaded}$ - $U_{Rs,loaded}$). R_m modifies the quality factor of the PCD antenna and it corresponds 0.375 Ω. As mentioned in previous sections a simplified depiction of an antenna is a parallel circuit where a capacitance is connected in parallel to an inductance and to its serial resistor. The PCD and the PICC are coupled through the mutual inductance M which changes its value depending on the position of the PICC. In order to get the mutual inductance M for each slot it is necessary to determine the S-parameters between PCD and PICC for each slot by measuring. Through these S-parameters the corresponding coupling coefficient k can be calculated. The increasing distance between PCD and PICC leads to decreasing of the coupling coefficient k. The simplified illustration of a chip corresponds as a parallel circuit of R_p and C_p. Through C_{tune} the resonance frequency of PICC can be adjusted to a certain value.

Determination of EMVCo PCD parameters: In order to implement the EMVCo equivalent circuit in LMA-Tool it was necessary to determine all the components of EMVCo PCD and PICC. The shunt resistance R_s and R_m are known values. The remaining EMVCo PCD components except the voltage source U_s were already determined by Christoph Egger during his thesis. Thus, these values were taken from his thesis. So far only the value of U_s and the values of k for each slot were unknown.

Known parameters:

- $R_s = 1\ \Omega$
- $R_m = 0.375\ \Omega$

Already determined parameters [1]:

Matching Circuit:

- $C_{ms} = 41.36$ pF
- $C_{mp} = 143$ pF

PCD Antenna:

- $R_1 = 0.766\ \Omega$
- $L_1 = 628$ nH
- $C_1 = 35.9$ pF

Unknown parameters:

- U_s
- k for the slots 0 to 4

The accuracy of all known PCD parameters is tested through Smith Chart (see figure 4.11) in order to investigate if they deliver 50 Ω at unloaded state. The parameters were adjusted as accurately as possible.

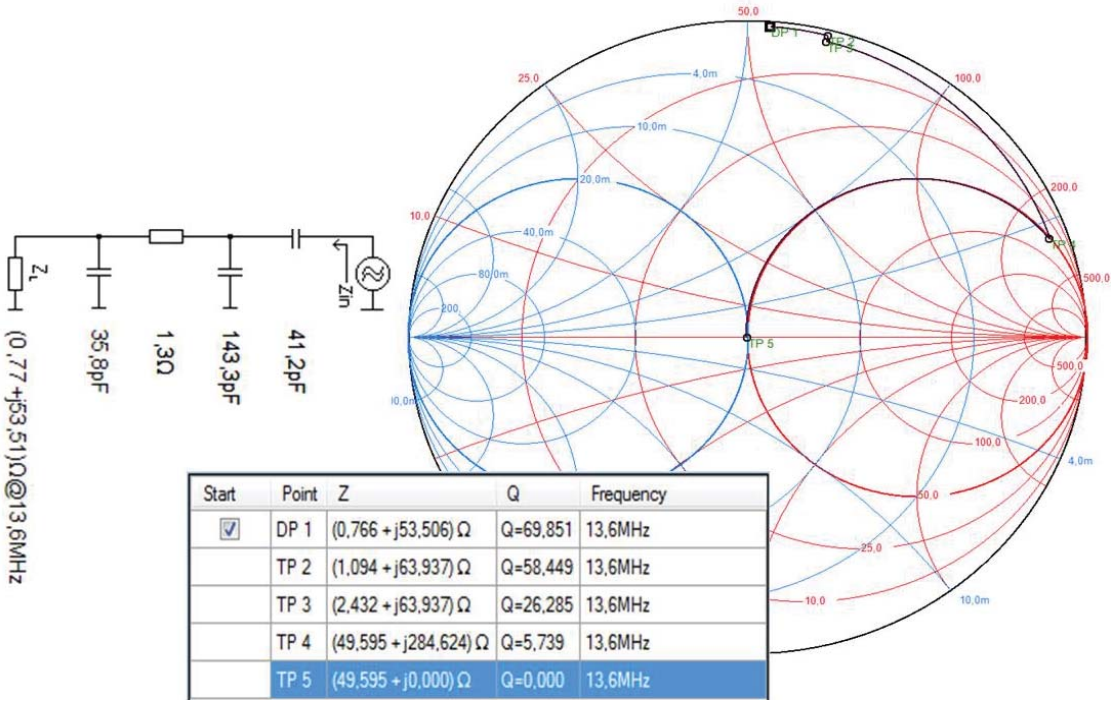

Figure 4.11: Smith Chart results with the determined values of Christoph Egger

Approach used to determine the voltage value of U_s:

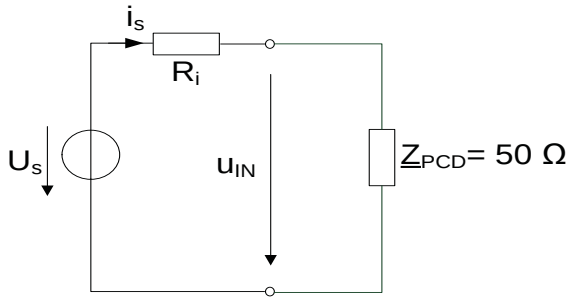

Figure 4.12: Corresponding equivalent circuit of PCD at antenna matching

The figure 4.12 shows the equivalent circuit of EMCo PCD, if the antenna matching at unloaded state is considered. By measuring u_{IN} at J2 SMA socket of EMVCo PCD at unloaded state, the voltage value of U_s can be calculated through the following simple calculations [8]:

$$\hat{u}_{IN,measured} = 7.935 \text{ V}$$

$$\hat{i}_s = \frac{\hat{u}_{IN,measured}}{\underline{Z}_{PCD}} = \frac{7.935V}{50\Omega} = 158.7mA \tag{4.2.1}$$

$$\hat{U}_s = \hat{i}_s \cdot R_i + \hat{u}_{IN,measured} = 158.7mA \cdot 50\Omega + 7.935V = 15.87V \tag{4.2.2}$$

Measured coupling coefficients for each slot and PICC antenna parameters:

- Slot 0: $k_{PCD,PICC} = 0.1781$
- Slot 1: $k_{PCD,PICC} = 0.1097$
- Slot 2: $k_{PCD,PICC} = 0.0707$
- Slot 3: $k_{PCD,PICC} = 0.0474$
- Slot 4: $k_{PCD,PICC} = 0.0329$

The coupling coefficient measurement was carried out with a Class 1 RefPICC (see figure 4.13). For the implementation in the LMA-Tool it was important to determine the antenna parameters of the reference PICC (RefPICC) through measuring [7].

- $L_{PICC} = 2.327\ \mu\text{H}$
- $R_{PICC} = 1.83\ \Omega$
- $C_{PICC} = 6.592$ pF

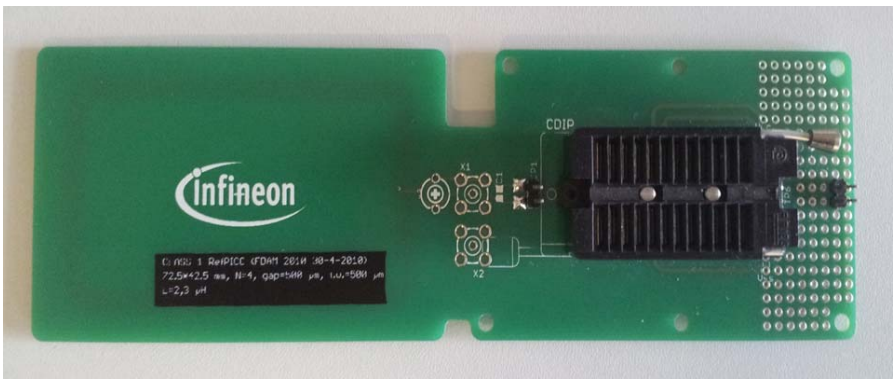

Figure 4.13: Class 1 RefPICC

Chapter 5: EMVCo estimation out of ISO measurement

After introductory information about ISO and EMV measurement the fifth chapter explains the main task of this thesis. This part of the thesis shows the approach used to get EMV related values out of ISO measurement.

The first step is a simple field strength sweep measurement with the ISO test assembly. This measurement delivers the differential voltage u_d (is proportional to i_2) and the voltage of the calibration coil u_{Cal} (corresponds to field strength) for each field strength point. With these voltage values the R_p and C_p values and the respective real power P_{real} of a chip are calculated through the LMA-Tool. The figure 5.1 shows the block diagram of the ISO set-up:

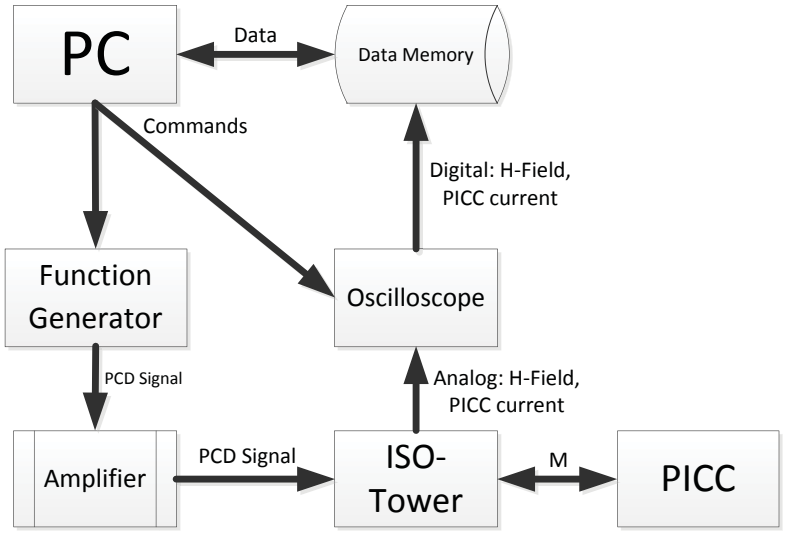

Figure 5.1: ISO-Measuring arrangement (adapted from [9])

The PC is responsible for the measuring procedure and serves as user interface. It is connected via GPIB (General Purpose Interface Bus) interface with a function generator and a digital oscilloscope. The PC transmits a predefined command to the function generator which passes on this signal over the amplifier to the ISO-tower. The function generator is connected with the amplifier by a BNC (Bayonet Nut Connector) cable because the output signal of the function generator is too low. Usually the amplifier and the ISO-tower are connected with each other by a SMA cable. The PICC to be measured is located on the center of the sense coil A of the ISO-tower. The ISO-tower delivers u_d and u_{Cal} which are digitalized by the oscilloscope and saved in the data memory [9].

In the following, the steps for a field strength sweep measurement of a chip are listed [9]:

- Tune the PICC to a specific resonance frequency
- Put the PICC on the ISO tower
- Measure signals with PIXIE measurement tool (LabVIEW tool of Infineon)
  - Calibrate the ISO set-up (error vector, field strength)
  - Define oscilloscope settings (trigger, time delay, duration)
  - Download a request command to the function generator for the correct type (type A or B)
  - Define field strength sweep (start, stop, step size)
  - Run automated data recording (save data in CSV format)
- Sort data to correct folder structure (see JH)

For each field strength point the voltages u_d and u_{Cal} are recorded as one CSV file. Through these CSV files the LMA-Tool calculates the values of R_p, C_p and P_{real}. LMA-Tool stands for *Load Modulation Analysis Tool* and is developed in MATLAB by Jürgen Hölzl. With these tool accurate analysis of ISO set-up, EMVCo set-up and additionally for generated data out of the simulation program *Advanced Design Systems ADS* is possible. Furthermore, a detailed single analysis of a modulated signal at a certain field strength point is achievable.

5.1 LMA-Tool Extension

It was essential to get acquainted with both standardized measurements in order to understand the main task of this thesis. Furthermore, it was highly important to roughly figure out the program sequence in order to extend the LMA-Tool to achieve the main goals of this thesis. For an accurate description of the program structure and functions of the LMA-Tool see the recommendation [9]. In this thesis only the parts of the LMA-Tool are mentioned, which were relevant for the main task and the extended part for EMVCo convergence.

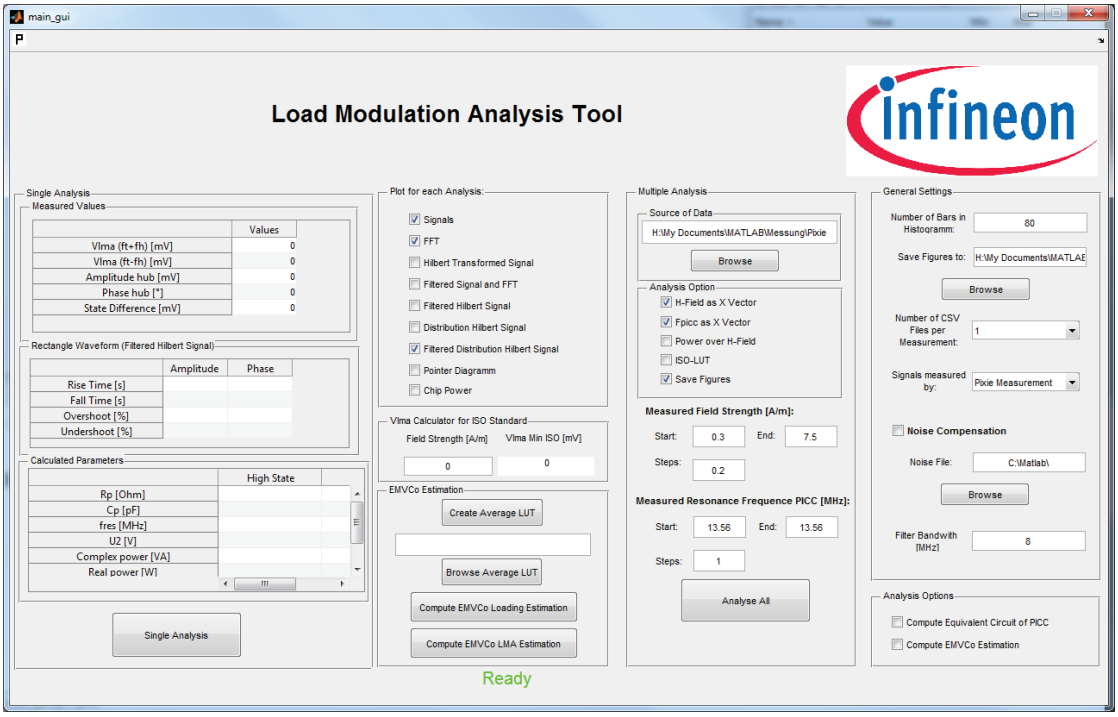

Figure 5.2: LMA Graphical User Interface

Defined directory structure:
As already mentioned the field strength sweep delivers the CSV files which has to be saved as in the following directory structure. The directory structure is retained as it was initially programed [9]:

- main folder (eg.: Measurement-2014-11)
  - sub folders: Chip name (eg.: Chip1)
    - sub sub folders: Resonance frequency (eg.: 13MHz, 15MHz, 17MHz)
      - in sub sub folders: Measured data files of field strength sweep (eg.: Chip1-1Am.csv, Chip1-2Am.csv, Chip1-3Am.csv)

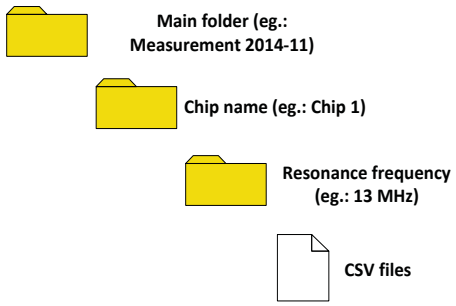

Figure 5.3: Directory structure

Creating a single ISO-LUT (Look Up Table): As the goal is to achieve an estimation of EMVCo values out of ISO measuring values it is crucial to constitute an ISO-LUT, which indicates the corresponding chip parameters for each field strength point within the adjusted field strength range. This table is created through the LMA-Tool. The ISO-LUT is essential for the iterative determination of EMVCo values. An accurate description of the iterative determination is explained in the next section.
The next step after creating the predetermined directory structure is to generate an ISO-LUT:

- Click the "Browse" button under the function *Multiple Analysis/Source of Data*
- Choose the main folder of the created directory structure
- Single out only the check box *ISO-LUT*
- Enter the *Start* and the *End* of measured field strength range with the according *Step*
  These is the same data which are adjusted in the PIXIE measurement tool
  Note: In this thesis only the field strength range 1 - 10 A/m with a step of 0.2 A/m is investigated!

- Type the adjusted resonance frequency of the PICC
- Click *Analyse All*
- A new directory *LUT* is created within the current folder and in this new directory the ISO-LUT is saved as an Excel file (.xls or .xlsx)

The steps listed above deliver one ISO-LUT for the corresponding field strength sweep measurement. It is important to mention that for each field strength sweep measurement with unchanged adjustment of the measuring devices (function generator, amplifier) and with unvaried position of the PICC the LMA-Tool delivers divergent values of R_p and C_p. One possible reason for this is that it is very difficult to get always exactly the same values of the PICC current $\underline{i}_2$ and its cause, namely the induced voltage $\underline{U}_{i,2}$ at one certain field strength point. By means of these two values the LMA-Tool calculates the chip parameters R_p and C_p.
Through multiple execution of the iterative determination with only one ISO-LUT it was observed that the implementation of the iterative determination by using only one single ISO-LUT is very tough to achieve. Thus an attempt with an average ISO-LUT out of five single ISO-LUTs was carried out. This approach delivered significantly improved results for the iterative determination. Therefore the field strength sweep measurement is performed five times in order to get an average ISO-LUT from five single ISO-LUTs.

Creating an average ISO-LUT: The following steps show how to get an average ISO-LUT through the LMA-Tool

- Click the ”Create Average LUT” button under the function *EMVCo Estimation*
- Double-click the *LUT* directory which is generated within the current folder
- Holding down the **Ctrl** key and select five single ISO-LUTs
- Click the ”Open” button
- An average ISO-LUT is created as an Excel file in the *LUT* directory

	H-Field[A/m]	Rp[Ohm]	Cp[F]	U2[V]	P_real[W]
1	1	774.2367	3.1023e-11	3.3008	0.0132
2	1.2000	952.3027	3.2104e-11	4.3972	0.0226
3	1.4000	700.3823	3.2728e-11	4.6576	0.0318
4	1.6000	519.8593	3.3514e-11	4.6339	0.0407
5	1.8000	437.0155	3.4055e-11	4.7057	0.0496
6	2	370.1002	3.5160e-11	4.6991	0.0582
7	2.2000	321.5768	3.6626e-11	4.6760	0.0666
8	2.4000	283.3315	3.8302e-11	4.6114	0.0749
9	2.6000	255.9575	3.9671e-11	4.5930	0.0831
10	2.8000	241.5356	4.0350e-11	4.6973	0.0911
11	3	219.2801	4.2357e-11	4.6273	0.0990
12	3.2000	205.7794	4.3813e-11	4.6498	0.1067
13	3.4000	191.6041	4.5696e-11	4.6560	0.1143
14	3.6000	184.6302	4.6913e-11	4.7413	0.1218
15	3.8000	178.3865	4.7780e-11	4.8483	0.1292
16	4	166.7438	5.0709e-11	4.7614	0.1365

Figure 5.4: Average ISO-LUT out of five single ISO-LUTs

Figure 5.4 shows only half of the entire average ISO-LUT. The first column displays the field strength points which increase with a step of 0.2 A/m. The start value of the field strength was chosen 1 A/m as the chips usually receive enough energy in order to communicate with the PCD at this field strength value. By means of the next column it can be seen that the R_p approximately achieves its maximum value at 1.2 A/m and then decreases monotonically with increasing field strength. Whereas C_p is inversely proportional to R_p and its values increase with increasing field strength. Through these behaviour of R_p and C_p (see figures 5.5 and 5.6) a constant voltage supply of the chip is achievable. The fourth column corresponds the supply voltage $\underline{U}_2$ of the chip. This column illustrates how the values of $\underline{U}_2$ stays almost constant with increasing field strength. The last column of the ISO-LUT is very essential for the iterative approach of EMVCo values. For the implementation of the iterative approach it was necessary to find a reference value which increases monotonically. Thus it is possible to assign a value to each field strength point and its corresponding R_p-C_p pair. For a clear and correct mapping of reference values to the corresponding R_p-C_p pair it is also significant that the determined curves of R_p and C_p have no increases. This is almost achieved through the average ISO-LUT. The first consideration was to realize the iterative determination by $\underline{U}_2$ but then it was noticed that $\underline{U}_2$ stays almost constant from 1 A/m on until 7.5 A/m. Therefore the real power P_{real} of the chip was investigated in order to figure if it increase

monotonically. The calculations of P_{real} had shown that it fulfills the required property namely it increases monotonically within the operating field strength range. The fifth column shows this result.

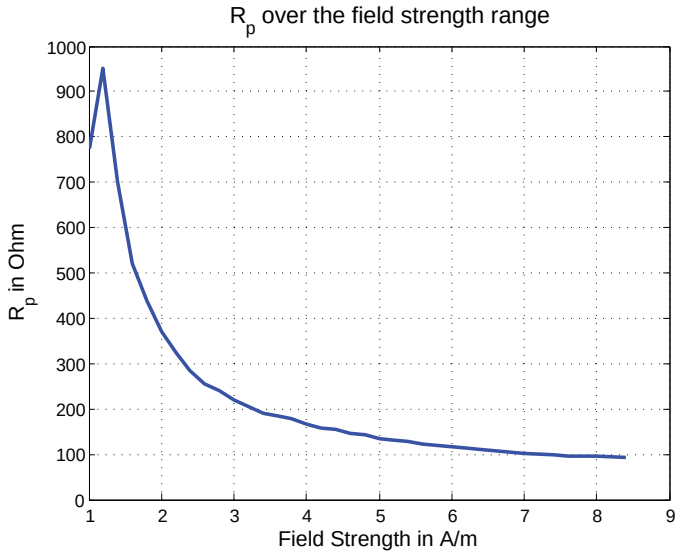

Figure 5.5: R_p curve of average ISO-LUT over the field strength range

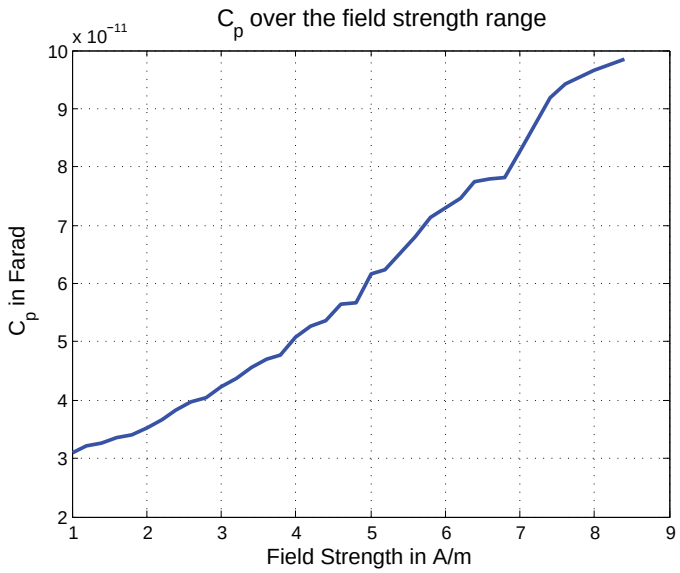

Figure 5.6: C_p curve of average ISO-LUT over the field strength range

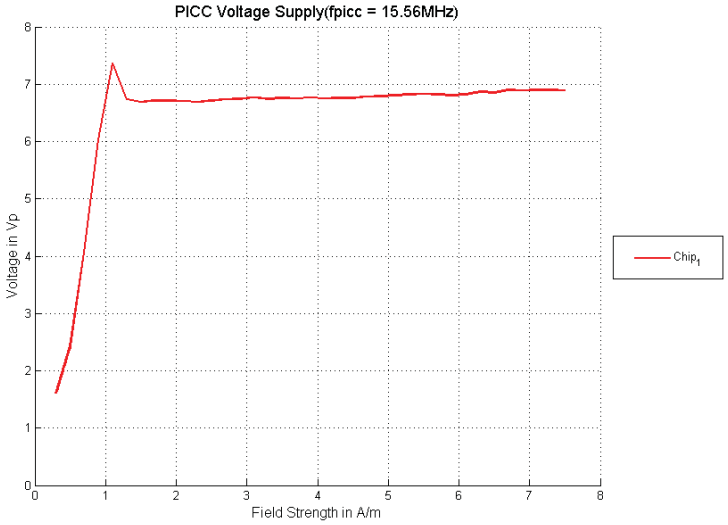

Figure 5.7: Voltage supply of the chip [9]

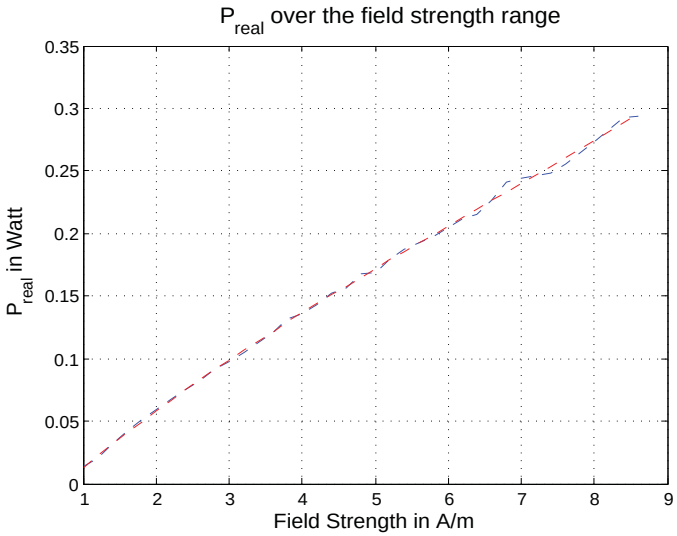

Figure 5.8: P_{real} curve of average ISO-LUT over the field strength range

The red dashed line in figure 5.8 illustrates the interpolated curve of P_{real}. Thus the increases of the calculated P_{real} values are prevented and also the curve is improved for the iterative determination.

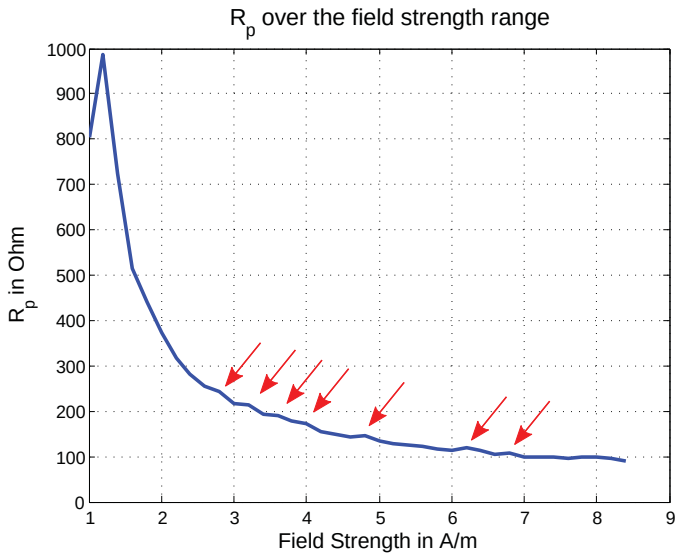

Figure 5.9: R_p curve of a single ISO-LUT

The red arrows in the figure 5.9 indicate to the increases in the curve.

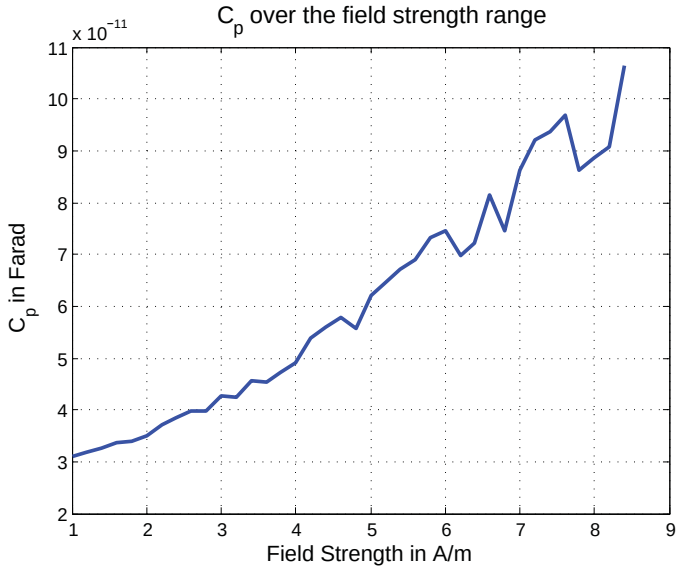

Figure 5.10: C_p curve of a single ISO-LUT

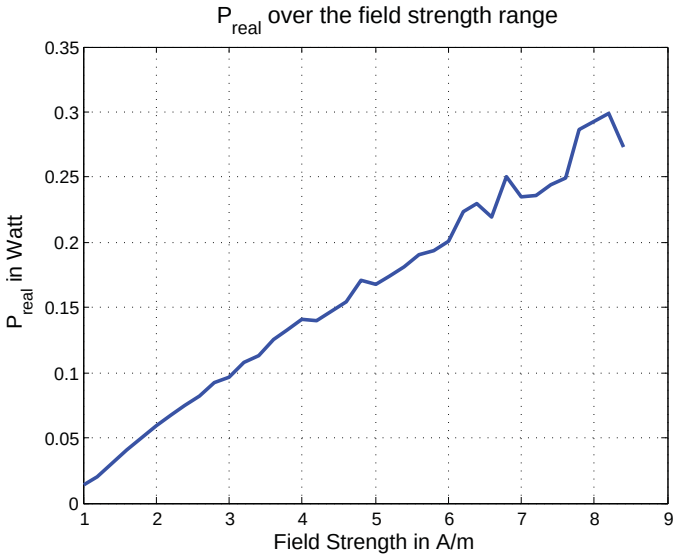

Figure 5.11: P_{real} curve of a single ISO-LUT

It was observed that it is very important to prepare the 'correct' LUT in order to implement the desired gradual determination of the EMVCo values. As previously mentioned, this means that it is required that the determined curves of R_p, C_p and P_{real} have no increases because thus the implementation of the gradual approach is almost impossible. Through generating of an average ISO-LUT it was noticed that these increases are reduced or ideally no increases appear (see figures 5.5, 5.6 and 5.8). The curves generated through only a single ISO-LUT which contain increases are depicted in the figures 5.9, 5.10 and 5.11 in order to show the difference between the curves of an average ISO-LUT and the curves of a single ISO-LUT.

The following tables show the behaviour of R_p within a measurement series consisting of five individual field strength measurements at five different arbitrary chosen field strength points. It lasted few minutes between two individual field strength measurements and approximately few hours between two measurement series. It was detected that the determined values of R_p at a certain field strength point and for repeated measurement have divergent values. Thus the following measurement series was performed in order to investigate how strongly the R_p values deviate between individual measurements and between each measurement series at certain field strength points.

	Field Strength Points				
	1 A/m	1.6 A/m	5 A/m	7.6 A/m	10 A/m
	$R_p[\Omega]$	$R_p[\Omega]$	$R_p[\Omega]$	$R_p[\Omega]$	$R_p[\Omega]$
1.Measurement	792.017	516.364	132.437	95.893	83.958
2.Measurement	758.957	512.417	140.562	96.462	83.732
3.Measurement	759.138	539.203	133.253	101.974	83.873
4.Measurement	757.049	516.323	133.132	95.948	88.539
5.Measurement	804.021	514.988	133.287	95.721	88.105
Average	774.237	519.859	134.534	97.199	85.642
Standard Deviation	22.136	10.932	3.387	2.683	2.454

Table 5.1: Investigation of R_p values within the first measurement series

	Field Strength Points				
	1 A/m	1.6 A/m	5 A/m	7.6 A/m	10 A/m
	$R_p[\Omega]$	$R_p[\Omega]$	$R_p[\Omega]$	$R_p[\Omega]$	$R_p[\Omega]$
1.Measurement	916.271	652.685	144.736	100.982	82.623
2.Measurement	1023.568	554.097	153.796	103.754	79.048
3.Measurement	904.065	641.65	143.051	94.871	81.616
4.Measurement	926.516	613.697	143.767	104.199	81.626
5.Measurement	968.482	617.698	154.534	96.375	83.013
Average	947.781	615.965	147.977	100.036	81.585
Standard Deviation	48.807	38.223	5.686	4.246	1.545

Table 5.2: Investigation of R_p values within the second measurement series

	Field Strength Points				
	1 A/m	1.6 A/m	5 A/m	7.6 A/m	10 A/m
	$R_p[\Omega]$	$R_p[\Omega]$	$R_p[\Omega]$	$R_p[\Omega]$	$R_p[\Omega]$
1.Measurement	1025.126	685.044	158.272	100.872	78.091
2.Measurement	999.855	623.686	142.281	95.84	87.442
3.Measurement	954.707	629.856	143.897	101.796	86.734
4.Measurement	947.317	627.965	152,606	111.551	78.397
5.Measurement	1000.037	633.445	151.772	102.278	78.126
Average	985.408	639.999	149.766	102.467	81.758
Standard Deviation	33.142	25.425	6.612	5.689	4.873

Table 5.3: Investigation of R_p values within the third measurement series

The essential notice of this measurement statistics is that within one measurement series the R_p values deviate strongly at a small field strength points and the deviation decreases with increasing field strength. The reason for the strong deviation in the range of the field strength point 1 A/m can be explained by the shunt mechanism.
At small field strength the quality factor of the PICC has to be high in order to get enough energy out of the magnetic field of the PCD. A small field strength means small value of induced voltage in the PICC and simultaneously also too less supply voltage for the chip to operate. The quality factor is increased according to the formula 3.2.1 for unchanged values of R_2 and L_2 through increasing the value of R_L (combination of shunt resistor R_s and R_p). So R_L is increased until the chip has enough supply voltage to operate. The maximum value of R_L indicates that the chip has achieved the needed supply voltage. It was noticed that R_L achieves its maximum at approximately 1.2 A/m and from this point on R_L decreases in order to guarantee a constant supply voltage. R_L attains its maximum at different values, because it is depending on the induced voltage in the PICC. 10 A/m is actually outside the operating field strength range (between 1.5 A/m and 7.5 A/m), but it is also measured and investigated as it was necessary for gradual approximation of the EMVCo values.
The chip increases its H_{min} value approximately 0.1 A/m at a higher temperature. Thus, a further possible reason for the deviation of R_p could also be the self-heating of the chip and of the measuring devices.

The following graphics show the deviation of R_p at small field strength points:

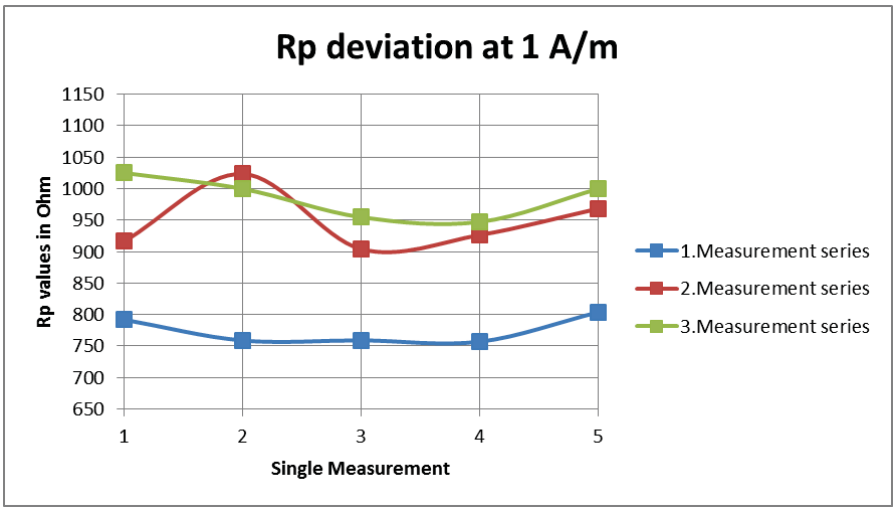

Figure 5.12: R_p deviation at 1 A/m

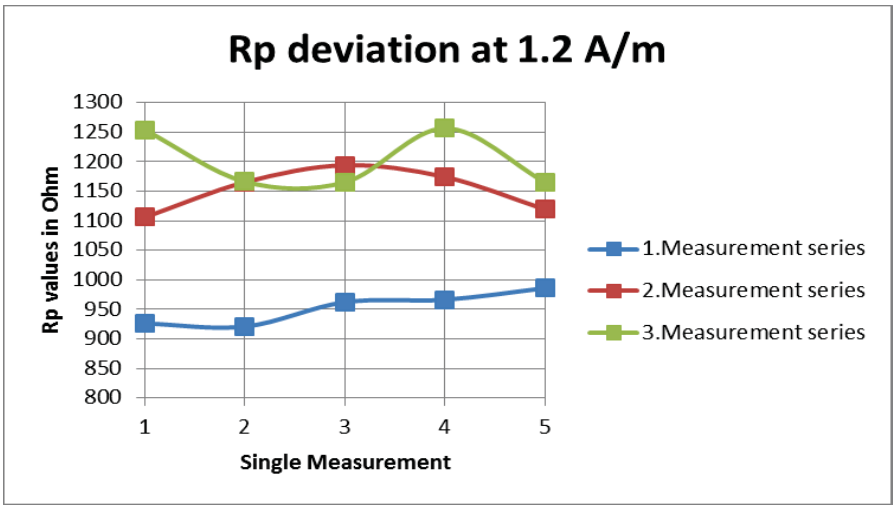

Figure 5.13: R_p deviation at 1.2 A/m

5.2 Iterative determination of EMVCo values

In order to start with the iterative determination it was necessary first to determine all EMCo PCD and PICC parameters and then to prepare an average ISO-LUT. The following simplified depiction shows the approach which was used for the iterative determination of EMVCo values out of ISO-measurement values. The figure 5.14 explains how the values of $R_{p,EMV}$ and $C_{p,EMV}$ are calculated for the respective slot in the operating volume of the EMV set-up. Through these values loading and LMA values for each slot of the operating volume are calculated.

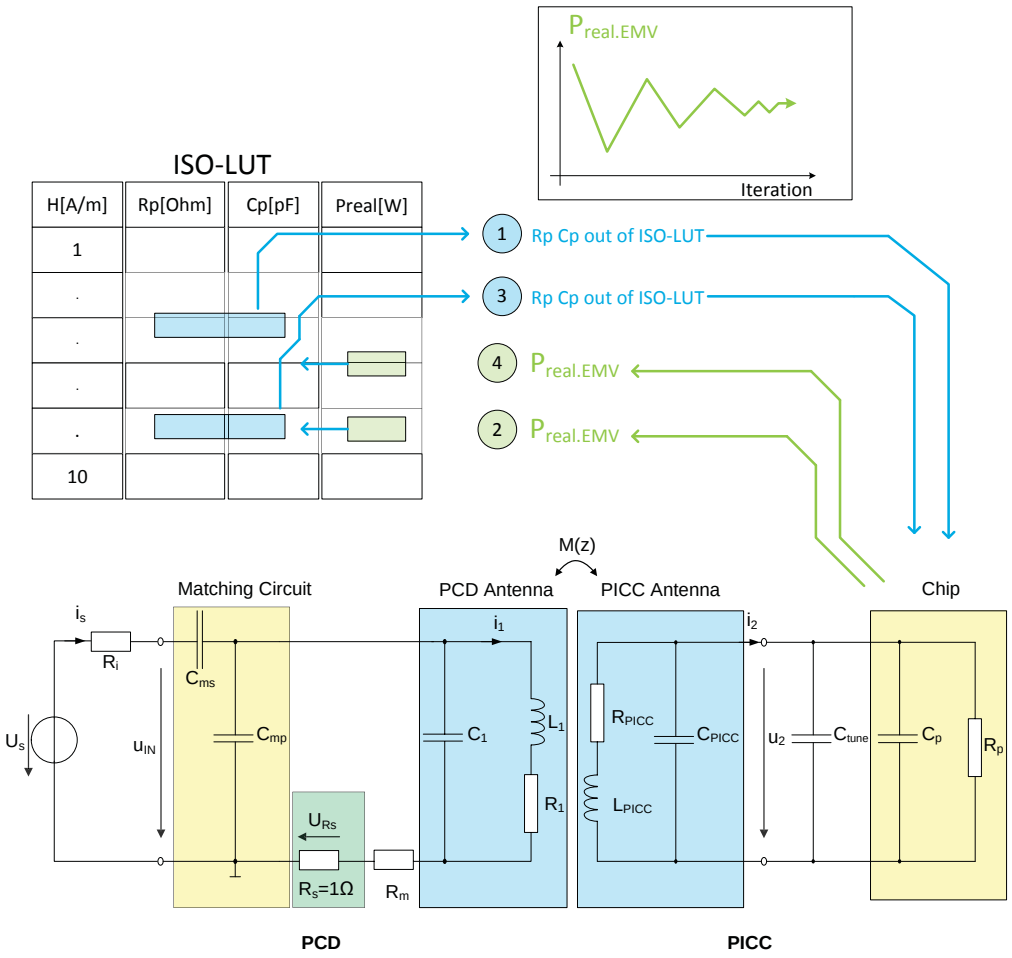

Figure 5.14: Approach in order to get EMVCo related values

The aim was to find out the approximate values of $R_{p,EMV}$ and $C_{p,EMV}$, which the chip would adjust in the different slots through the $R_{p,ISO}$ and $C_{p,ISO}$ values. The $R_{p,ISO}$ and $C_{p,ISO}$ values are determined for every field strength point within the selected field strength range (1 - 10 A/m and with 0.2 A/m steps). Thus the $R_{p,EMV}$ and $C_{p,EMV}$ values can be determined for the respective slot of the operating volume. In each slot a different field strength value is measured because of the different distance of the PICC to the PCD. With increasing distance from PCD the field strength value decreases. The different field strength values for each slot is described by the coupling coefficient k for the respective slot.

The iterative determination is achieved through the following five steps.

- 1.Step: Take the $R_{p,ISO}$ and $C_{p,ISO}$ values at the middle of the selected field strength range
- 2.Step: Use these both values in the EMVCo equivalent circuit for R_p and C_p and with these values calculate the real power $P_{real,EMV}$ of the chip.
- 3.Step: With the calculated $P_{real,EMV}$ determine the corresponding $R_{p,ISO}$ and $C_{p,ISO}$ through interpolation
- 4.Step: With the new determined $R_{p,ISO}$-$C_{p,ISO}$ pair, calculate $P_{real,EMV}$ for the next iteration
- 5.Step: Execute the third step again

This iteration is repeated until the curve shape of the calculated $P_{real,EMV}$ approximately corresponds to the curve shape which is depicted in figure 5.14 at the right top corner. The aim and the wish is that the calculated $P_{real,EMV}$ should level off to a constant value and so it indicates to the $R_{p,EMV}$-$C_{p,EMV}$ pair for the respective slot.
Next, the formulas are given which are used within the second step. In this iteration step the $P_{real,EMV}$ is calculated with $R_{p,ISO}$ and $C_{p,ISO}$ for the respective slot.

Transformed Impedance $\underline{Z'}_T$ 3.3.1:

$$\underline{Z'}_T = \frac{\omega^2 k^2 L_1 L_{PICC}}{R_{PICC} + j\omega L_{PICC} + \frac{R_P}{1+j\omega R_P(C_{PICC}+C_{Par})}}$$

Where for k the determined coupling coefficient value of the corresponding slot is inserted.

Calculation of the total EMVCo PCD impedance at loaded state:

$$\underline{Z}_1 = R_1 + j\omega L_1 + \underline{Z'}_T \tag{5.2.1}$$

$$\underline{Z}_2 = \frac{\underline{Z}_1}{1 + j\omega C_1 \underline{Z}_1} \tag{5.2.2}$$

$$\underline{Z}_3 = \underline{Z}_2 + R_m + R_s \tag{5.2.3}$$

$$\underline{Z}_4 = \frac{\underline{Z}_3}{1 + j\omega C_{mp} \underline{Z}_3} \tag{5.2.4}$$

$$\underline{Z}_{PCD,loaded} = R_i + \underline{Z}_4 + \frac{1}{j\omega C_{ms}} \tag{5.2.5}$$

Calculation of the PCD antenna current i_1 in order to determine the induced voltage $U_{i,PICC}$ in PICC:

$$\underline{i}_s = \frac{\hat{u}_s \cdot e^{j \cdot \varphi_{\hat{u}_s}}}{\underline{Z}_{PCD,loaded}} = \frac{\hat{u}_s \cdot e^{j \cdot 0}}{\underline{Z}_{PCD,loaded}} \tag{5.2.6}$$

In the counter of the formula 5.2.6 the phase of source voltage is set to 0 degree.

$$\underline{u}_{Z_4} = \underline{i}_s \cdot \underline{Z}_4 = \underline{i}_{R_s} \cdot (\underline{Z_2} + R_s + R_m) \tag{5.2.7}$$

$$\underline{i}_{R_s} = \frac{\underline{u}_{Z_4}}{\underline{Z_2} + R_s + R_m} \tag{5.2.8}$$

$$\underline{u}_{R_s} = \underline{i}_{R_s} \cdot R_s \tag{5.2.9}$$

$$\underline{u}_{Z_2} = \underline{u}_{Z_4} - \underline{i}_{R_s} \cdot (R_s + R_m) \tag{5.2.10}$$

$$\underline{i}_1 = \frac{\underline{u}_{Z_2}}{\underline{Z_1}} \tag{5.2.11}$$

$$\underline{u}_{i,PICC} = j\omega k \sqrt{L_1 \cdot L_{PICC}} \cdot \underline{i}_1 \tag{5.2.12}$$

Calculation of the current $\underline{i}_2$ and supply voltage $\underline{u}_2$ in order to determine the real power P_{real} of the chip:

$$\underline{i}_2 = \frac{\underline{u}_{i,PICC}}{R_{PICC} + j\omega L_{PICC} + \frac{R_P}{1+j\omega(C_{PICC}+C_P)R_P}} \tag{5.2.13}$$

$$\underline{u}_2 = \underline{i}_2 \cdot \frac{R_P}{1 + j\omega(C_{PICC} + C_P)R_P} \tag{5.2.14}$$

$$\underline{P}_{real} = \frac{1}{2} \cdot |\hat{\underline{i}}_2| \cdot |\hat{\underline{u}}_2| \cdot \cos\varphi \tag{5.2.15}$$

φ corresponds to the phase between $\underline{i}_2$ and $\underline{u}_2$ whereby $\underline{u}_2$ is also set to 0 degree.

With this determined value of P_{real} the R_p-C_p pair for the next iteration is determined through interpolation.

Results of the iterative determination:

Through the following steps the LMA-Tool delivers the curve shapes of $P_{real,EMV}$ for all slots of the operating volume:

- Click ”Browse Average LUT” under the function *EMVCo Estimation*
- Double-click the *LUT* directory and choose the already created average LUT
- Click ”Compute EMVCo Loading Estimation”

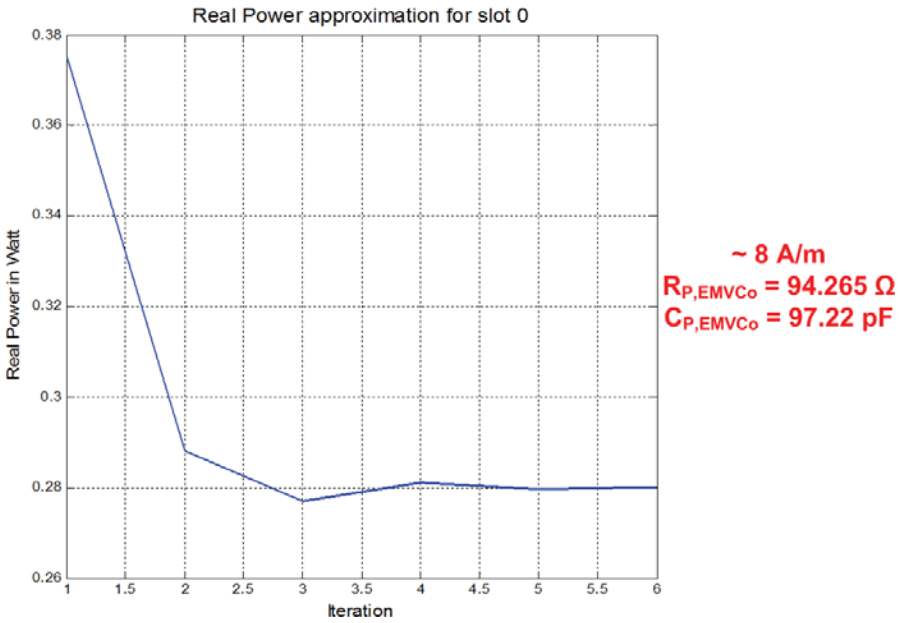

Figure 5.15: Curve shape of calculated $P_{real,EMV}$ in slot 0

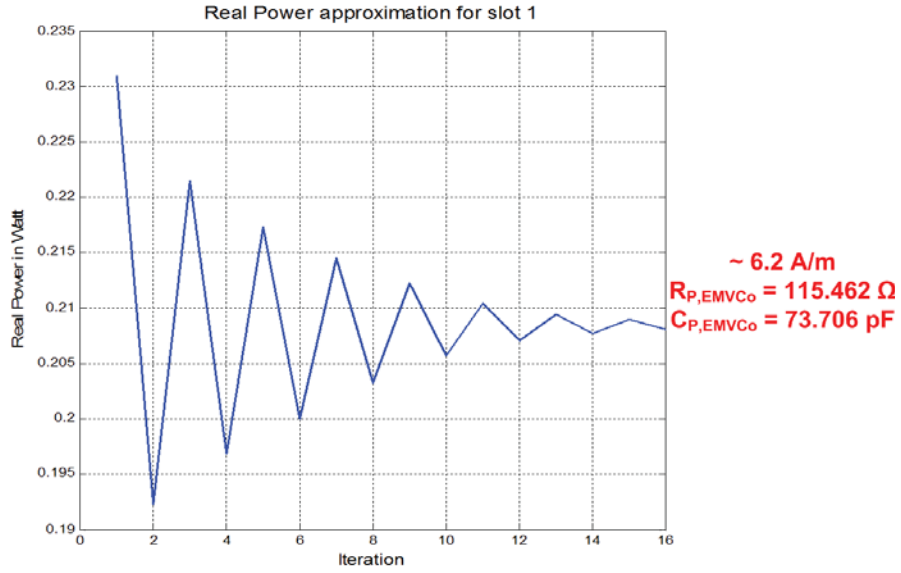

Figure 5.16: Curve shape of calculated $P_{real,EMV}$ in slot 1

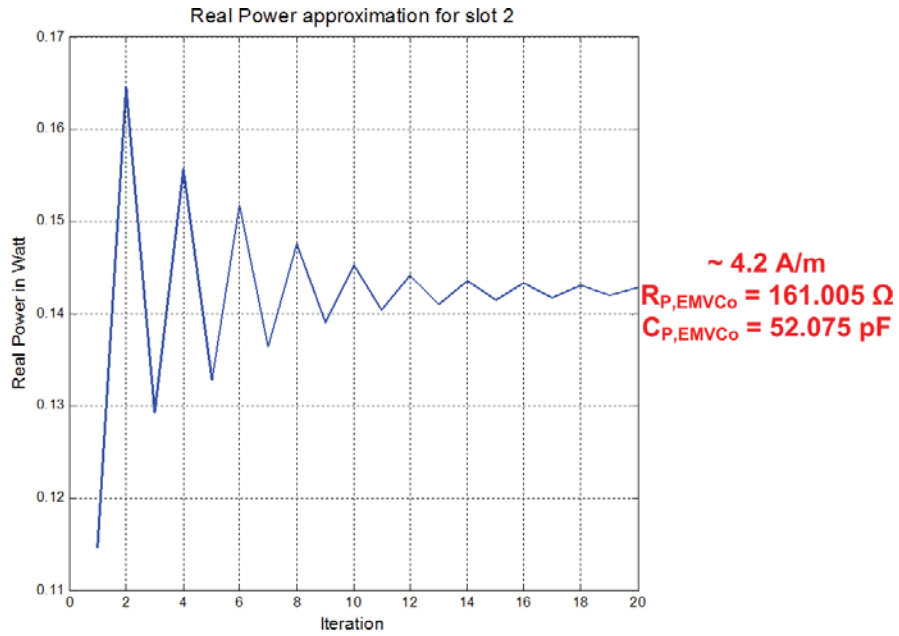

Figure 5.17: Curve shape of calculated $P_{real,EMV}$ in slot 2

Figure 5.18: Curve shape of calculated $P_{real,EMV}$ in slot 3

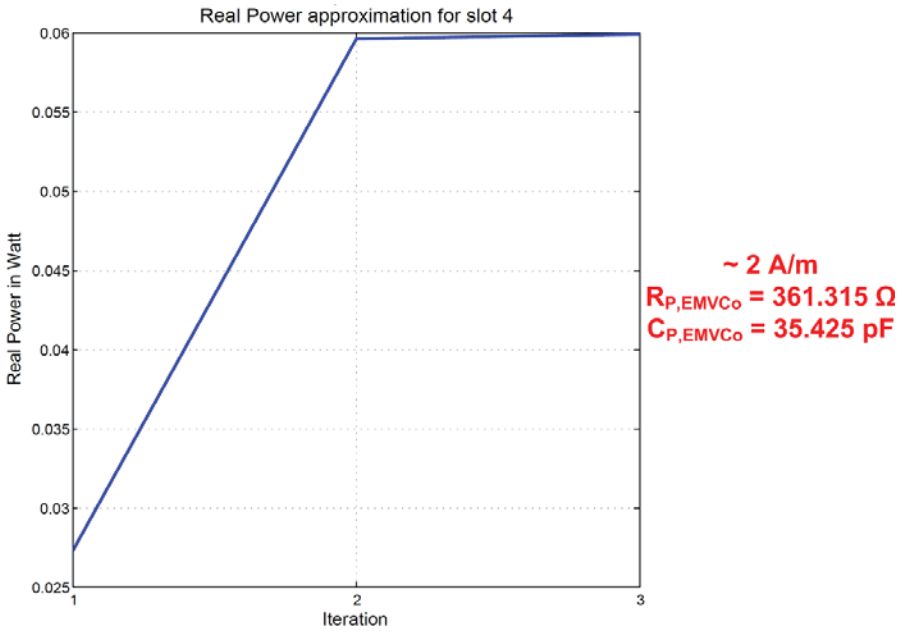

Figure 5.19: Curve shape of calculated $P_{real,EMV}$ in slot 4

5.3 Comparison of measurement results and LMA-Tool results

Loading and LMA values can be determined after the iterative determination of $R_{p,EMV}$ and $C_{p,EMV}$ for each slot. The first step was to compare the measured and the simulated loading values with each other in order to see how strong they differ from one another. As already briefly mentioned, loading is the difference between the voltage drop at shunt resistance U_{Rs} at unloaded state and the voltage drop at shunt resistance U_{Rs} at loaded state(Loading = $U_{Rs,unloaded}$ - $U_{Rs,loaded}$). At unloaded state the PICC is outside of the magnetic field of the PCD and this means that k equals zero thus the transformed impedance $\underline{Z'}_T$ corresponds also to zero (see formula 3.3.1). At loaded state the PICC is within the magnetic field of the PCD and therefore the feedback effect of the PICC to the antenna current i_1 through $\underline{Z'}_T$ has to be taken into account. The following tables show the measured and simulated loading values for all slots at the positions (z,0,0) (see chapter 4.2.1.2).

Measurement

$\hat{U}_{Rs,unloaded} = 0.712$V	
Loaded	
Slot number	$\hat{U}_{Rs}[V]$
Slot 0	0.621
Slot 1	0.668
Slot 2	0.68
Slot 3	0.687
Slot 4	0.693

(a)

LMA-Tool

$\hat{U}_{Rs,unloaded} = 0.714$V	
Loaded	
Slot number	$\hat{U}_{Rs}[V]$
Slot 0	0.564
Slot 1	0.635
Slot 2	0.669
Slot 3	0.686
Slot 4	0.697

(b)

Table 5.4: $\hat{U}_{Rs}$ values of Measurment and LMA-Tool at unloaded and loaded state

Measurement

$\hat{U}_{Rs,unloaded} = 0.712$V	
Loaded	
Slot number	Loading[%]
Slot 0	12.78
Slot 1	6.18
Slot 2	4.49
Slot 3	3.51
Slot 4	2.67

(a)

LMA-Tool

$\hat{U}_{Rs,unloaded} = 0.714$V	
Loaded	
Slot number	Loading[%]
Slot 0	21.06
Slot 1	11.12
Slot 2	6.26
Slot 3	3.85
Slot 4	2.34

(b)

Table 5.5: Loading values of Measurment and LMA-Tool are given as percentage

The measurement and the LMA-Tool with the determined parameters of PCD and PICC (see 4.2.2) deliver for $\hat{U}_{Rs,unloaded}$ almost the same values with only a minimal deviation form one another. In the table 5.4 it can be seen that at slot 0 the simulated $\hat{U}_{Rs,unloaded}$ value deviates most strongly from the measured $\hat{U}_{Rs,unloaded}$ value. In the remaining slots the $\hat{U}_{Rs,unloaded}$ values determined by the LMA-Tool almost exactly match with the measured values. Nevertheless the table 5.5 shows that the loading values in percentage terms strongly differ from one other. Noticeable is that the percentage loading values of LMA-Tool in the first two slots are approximately twice as high as the measured values. The strong deviation at slot 0 led to an error search in order to improve the simulated loading values especially of slot 0. Therefore, the PCD antenna parameters and the coupling coefficients were measured again. Additionally, slot 0 was investigated whereby

the loading at slot 0 was measured and simulated with passive components instead of a chip. Thus concrete and known values are added for R_p and C_p for the simulation with ADS.

5.3.1 EMV PCD Antenna Measurement

Usually the EMV PCD antenna parameters are determined with an impedance and network analyzer as follows [7]:

- PCD antenna parameters are already approximately known and in order to measure the PCD antenna in the range of 13.56 MHz the capacity has to be calculated for this frequency with the following formula:

$$f_{res} = \frac{1}{2\pi\sqrt{L_1(C_{add} + C_1)}} \tag{5.3.1}$$

$$(C_{add} + C_1) = \frac{1}{L_1(2\pi f_{res})^2} \tag{5.3.2}$$

  If the already known capacity C_1 is subtracted from the calculated sum of $C_{add}+C_1$ then the additional capacity C_{add} can be determined in order to measure the PCD antenna parameters in the range of 13.56 MHz

- EMV PCD antenna is measured with an additional capacity C_{add}
- The impedance and network analyzer delivers the measured sum of $C_{add} + C_1$ and through subtracting C_{add} the actual capacity value of the EMV PCD antenna can be determined.
- The resistance R_1 and the inductance L_1 of the PCD antenna can be read off from the measuring device

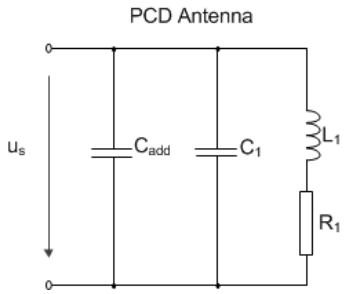

Figure 5.20: Additional capacity is necessary for the measurement

The following tables show the measurement results, whereby the PCD antenna was measured once with an SMA cable and once directly at the measuring device. The duration between two single measurements lasted few minutes.

Measurement with SMA cabel

$R_1[m\Omega]$	$C_1[pF]$	$L_1[nH]$
611.03	39.08	609.08
602.88	38.3	606.28
608.81	38.7	605.13
605.41	37.84	607.56
603.13	38.23	606.44

(a)

Measurement at measuring device

$R_1[m\Omega]$	$C_1[pF]$	$L_1[nH]$
619.02	36.34	609.56
619.79	36.39	609.4
619.32	36.48	609.19
620.3	36.42	609.32
619.38	36.46	609.17

(b)

Table 5.6: EMV PCD antenna parameter measurement

The comparison of the resistance values of both methods shows that they fairly differ from one another whereby the capacity values and inductance values deviate quite minimal from one other. In contrast to the measurement with cable, the table 5.6b shows that the measurement values without cable remain quite constant. Noticeable is that the new measured EMV PCD antenna parameters of both methods, also strongly differ from the determined values by Christoph Egger. For further investigation the first measured values of method b were used and simultaneously they were checked through curve fitting in ADS.

In the following, the measurement and the simulation curve of EMV PCD antenna are compared.

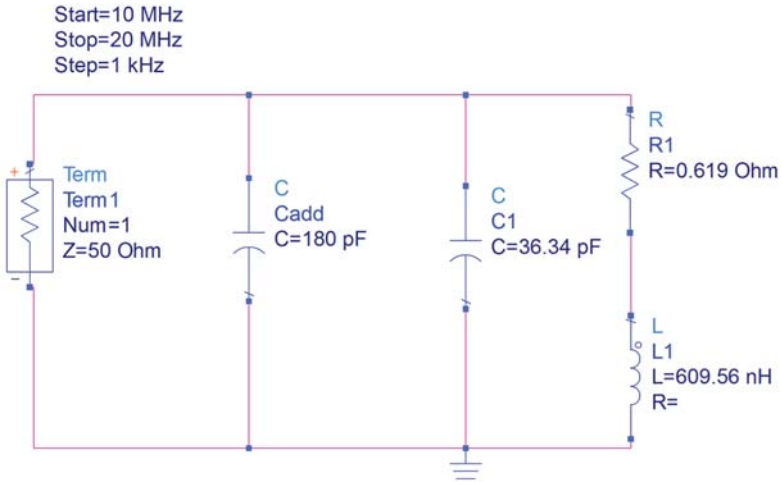

Figure 5.21: Simulation of EMV PCD antenna with C_{add}

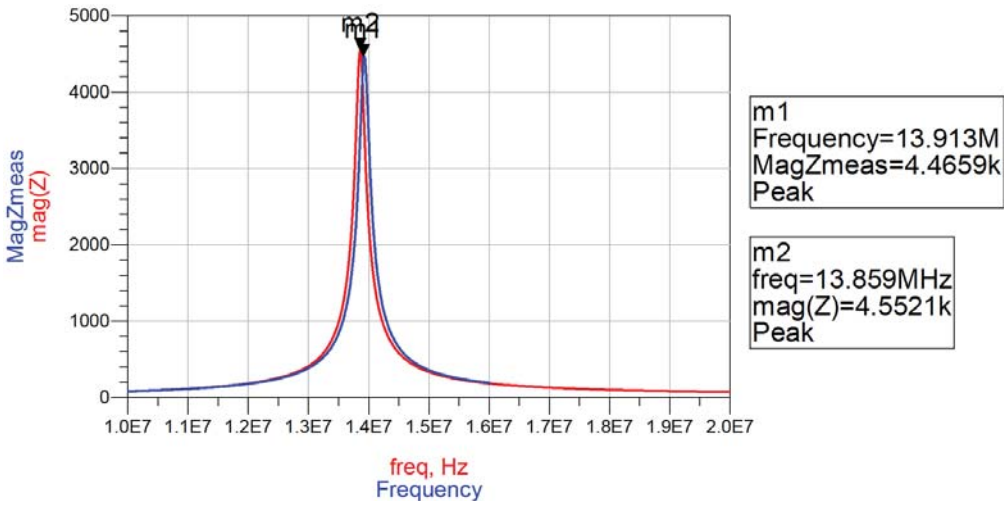

Figure 5.22: Impedance curve of measured and simulated EMV PCD antenna with C_{add}

The blue curve illustrates the measured curve with the marker $m1$ and the red curve corresponds to the simulated curve with the marker $m2$. In order to achieve an accurate measurement a COG capacitor was used. According to the curve fitting in figure 5.22 it can be said that the new measured EMV PCD antenna parameters with C_{add} are quite well determined. An accurate fitting of both curves was possible through fine-tuning of antenna parameters:

- $R_{1,adjusted}$=0.6358Ω
- $C_{1,adjusted}$=34.69 pF
- $L_{1,adjusted}$=609.56 nH

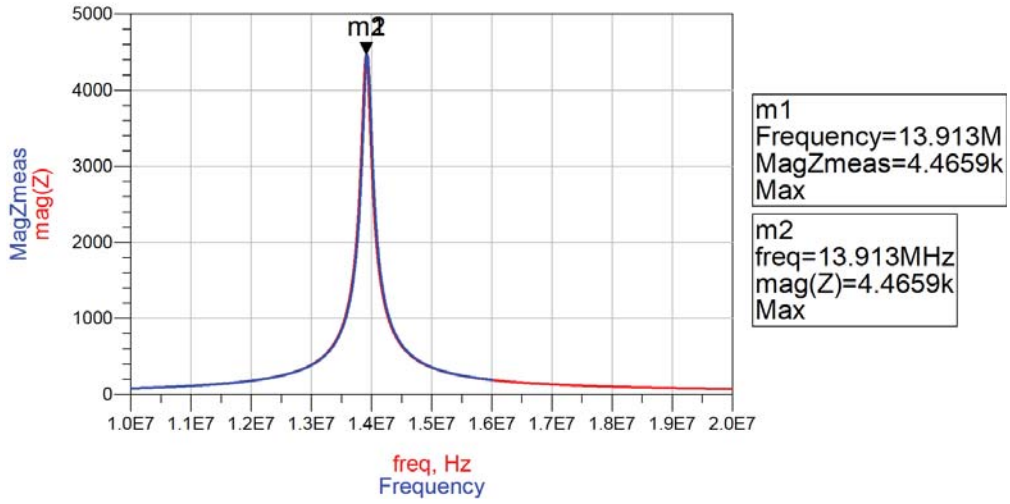

Figure 5.23: EMV PCD antenna: Simulated curve fitted with measured curve

It was also interesting to examine the same measurement without an additional capacity in order to find out if it is also possible to determine quite accurately the antenna parameters in a higher frequency range. The following figures show the result of the EMV PCD antenna measurement but without C_{add}.

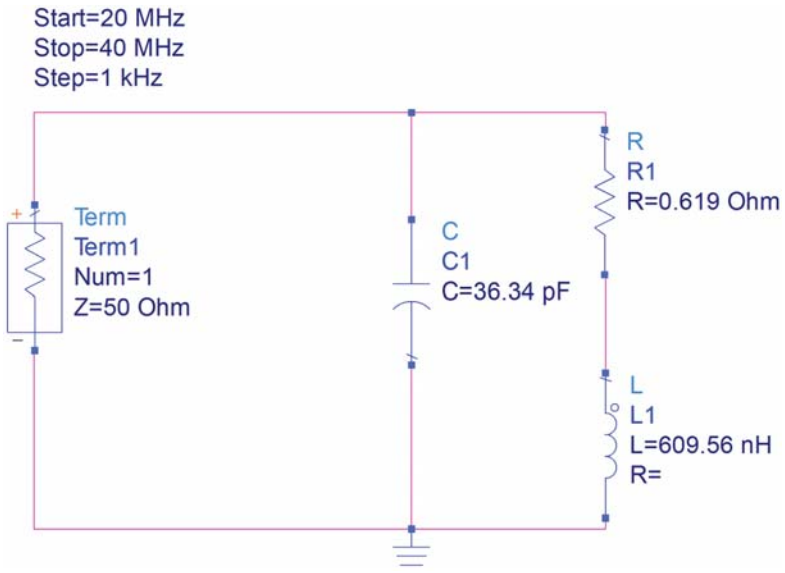

Figure 5.24: Simulation of EMV PCD antenna without C_{add}

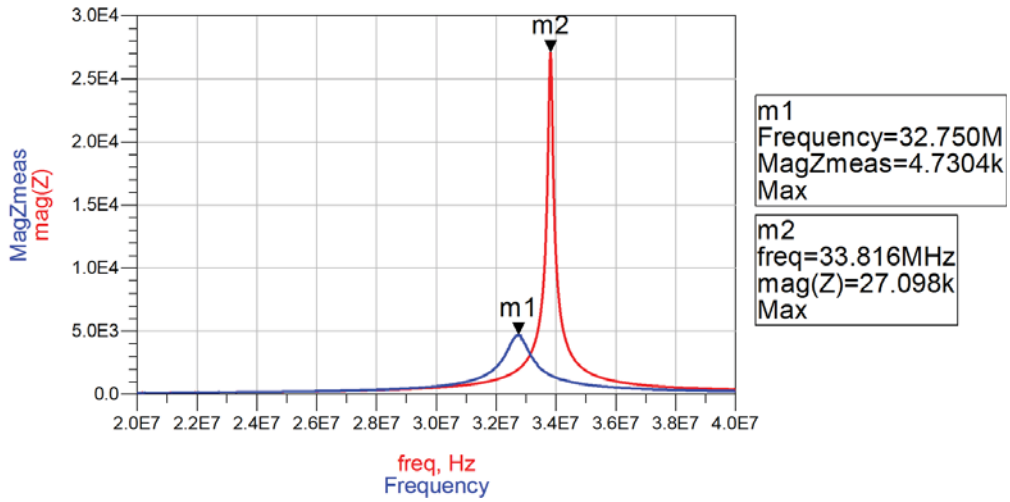

Figure 5.25: Measured and simulated curve of EMV PCD antenna without C_{add}

Through figure 5.25 the significant mismatch between the measured curve (blue) and the simulated curve (red) can be seen clearly. Especially the quality factor of the simulated curve is higher than the measured curve. The simulated curve was almost fitted to the measured curve with the following antenna parameters:

- $R_{1,adjusted}$=3.4353Ω
- $C_{1,adjusted}$=38.14 pF
- $L_{1,adjusted}$=619.56 nH

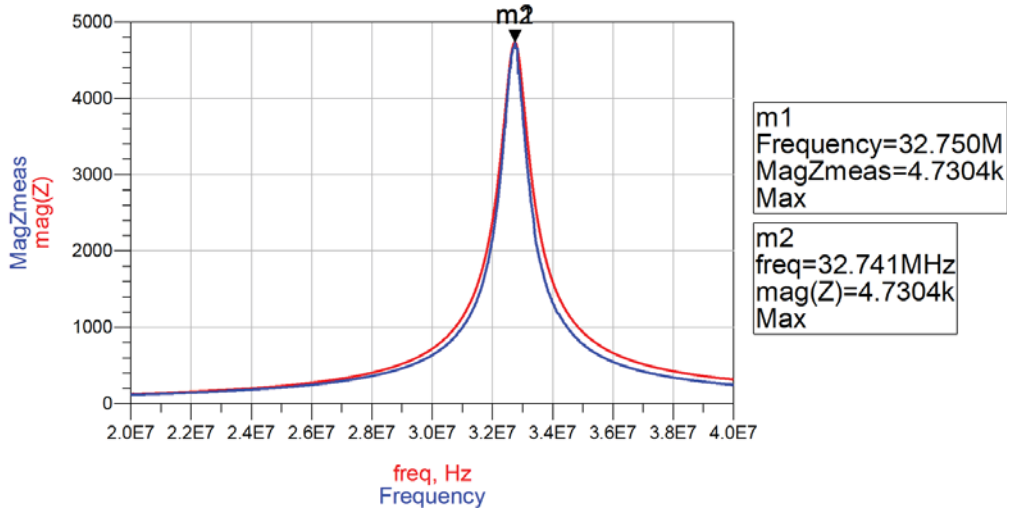

Figure 5.26: EMV PCD antenna: Simulated curve almost fitted with measured curve

The resistance R_1 had to be significantly increased in order to achieve a matching between both curves. But the adjusted antenna resistance in the simulation is too high for such an EMV PCD antenna and it does not approximately correspond the actual value. The EMV PCD antenna measurement without C_{add} shows that the simulated curve and the measured curve noticeable differ from one other whereby the same measurement with C_{add} and without fine-tuning already delivers clearly better curve fitting of both curves.

5.3.2 Measurement of coupling coefficient k

The coupling coefficient k could be also a further possible cause of a strong deviation between measured loading value and simulated loading value by LMA-Tool at slot 0. Therefore k was measured again for each slot in order to investigate the deviation of the measured values for repeated measurements. The following table shows the measured values of k for the corresponding slots.

	1.Measurement	2.Measurement	3.Measurement
Slot number	$k_{PCD,PICC}$	$k_{PCD,PICC}$	$k_{PCD,PICC}$
0	0.1781	0.1785	0.1782
1	0.1097	0.1075	0.1077
2	0.0707	0.0694	0.0692
3	0.0474	0.0467	0.0467
4	0.0329	0.0325	0.0325

Table 5.7: Measurement series of coupling coefficient k measurement

This measurement series had shown that the measured values of k for a certain slot deviate slightly from one other. Especially the determined k values for slot 0 vary in the fourth position after the decimal point. Thus it can be assumed that the measured values are quite well determined. A further investigation was also done with a special simulation program (HFSS) which determined again k for slot 0. Additionally, the position of the PICC was varied within the slot 0 in order to find out how strong the value of k varies at minimal change in position of the PICC.

The figure 5.27 shows the simplified layout plane of the operating volume and the RefPICC. If the antenna of the RefPICC (see figure 4.13) is completely inside the slot then x corresponds 0. For the simulation the x axis was varied between -1 mm and 1 mm and y axis, which should correspond the distance between the PCD antenna and the RefPICC, was varied between 14 mm and 16 mm.

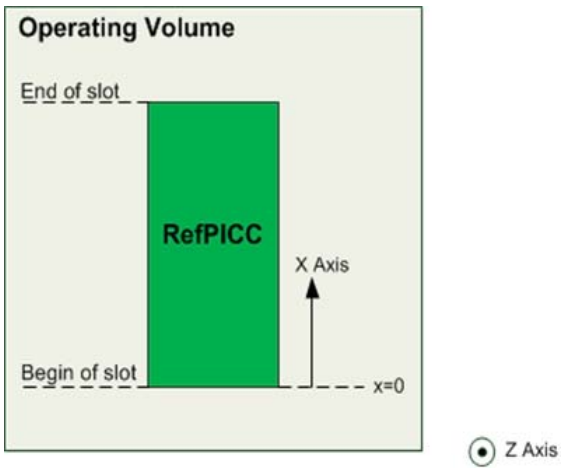

Figure 5.27: Simplified floor plan view of the operating volume and the RefPICC

The following table 5.8 shows the results of k for slot 0 which were determined by HFSS and additionally the respective percentage deviation from the average value (0.1783) of the measured coupling coefficients at slot 0 . Through this simulation results it can be said that the measured k values of slot 0 approximately correspond the simulated k values at y = 16 mm. Furthermore, a minimal variation of the RefPICC position in x direction leads to a slight deviation of k whereas a small variation of the distance between PCD and RefPICC results in a significantly greater deviation of the k values. According to the simulation values it can be argued that an accurate measurement of k is very difficult because already a little variation of the RefPICC position within a slot leads to a different value of k. Additionally, the measurement deviations through measurement devices and measurement cables should also be considered.

	Coordinates of RefPICC		
	x = -1 mm, y = 14 mm	x = 0 mm, y = 14 mm	x = 1 mm, y = 14 mm
$k_{PCD,PICC}$	0.2097 (+17.6%)	0.2096 (+17.6%)	0.2093 (+17.4%)

	x = -1 mm, y = 15 mm	x = 0 mm, y = 15 mm	x = 1 mm, y = 15 mm
$k_{PCD,PICC}$	0.1989 (+11.6%)	0.199 (+11.6%)	0.1986 (+11.4%)

	x = -1 mm, y = 16 mm	x = 0 mm, y = 16 mm	x = 1 mm, y = 16 mm
$k_{PCD,PICC}$	0.1887 (+5.8%)	0.1888 (+5.8%)	0.1881 (+5.5%)

Table 5.8: Simulation results of k for slot 0

5.3.3 Curve fitting

By means of curve fitting, the measured and the related simulation curve shapes of the RefPICC and EMV PCD were compared. Through this method it can be seen if the measurement results of each part approximately correspond with its simulation results. Thus the mismatch between measurement and simulation (thus also LMA-Tool) will be figured out. Both parts, RefPICC and EMV PCD, were investigated separately.

5.3.3.1 Curve fitting of RefPICC

First, the accuracy of the measured RefPICC antenna parameters (see page 41) is examined through curve fitting. Also the antenna of the RefPICC was measured and simulated with C_{add} in order to depict the curves in the range of 13.56 MHz.

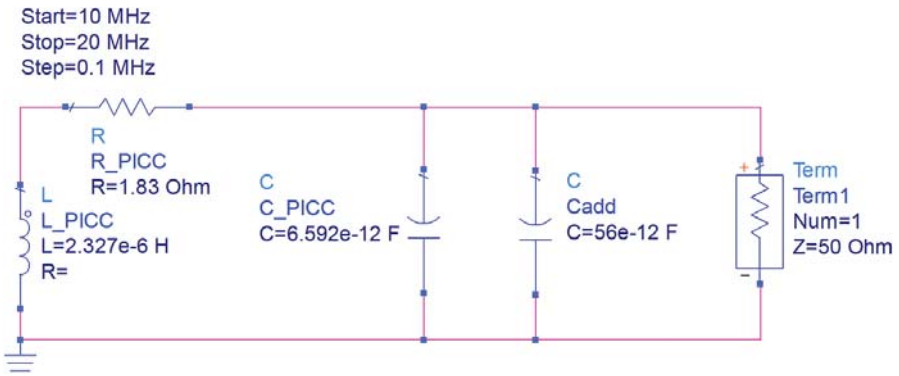

Figure 5.28: Simulation of RefPICC antenna with C_{add}

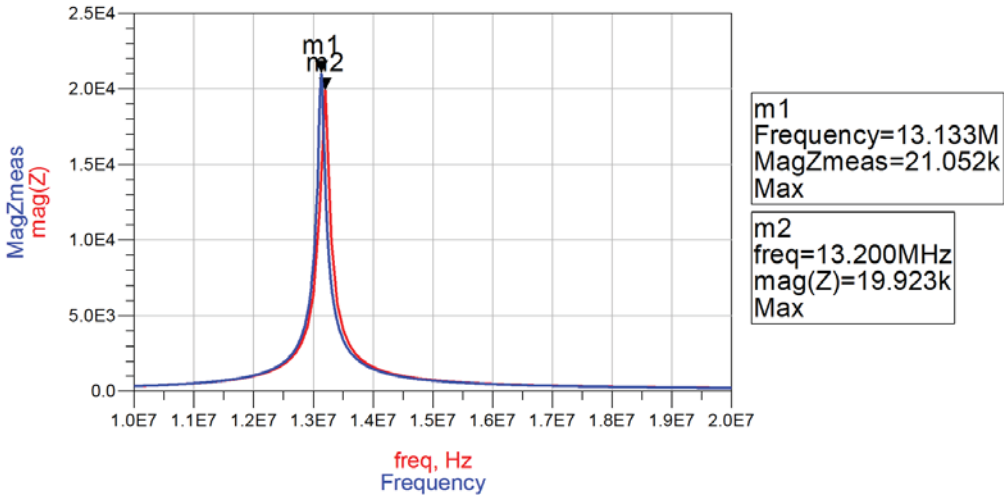

Figure 5.29: Impedance curve of measured and simulated RefPICC antenna

Regarding the figure 5.29 it can be argued that the measured RefPICC antenna parameters were quite well determined. With fine-tuning of these parameters, a better matching of both curves was possible.

- $R_{PICC,adjusted} = 1.397\ \Omega$
- $C_{PICC,adjusted} = 7.082$ pF
- $L_{PICC,adjusted} = 2.327$ uH

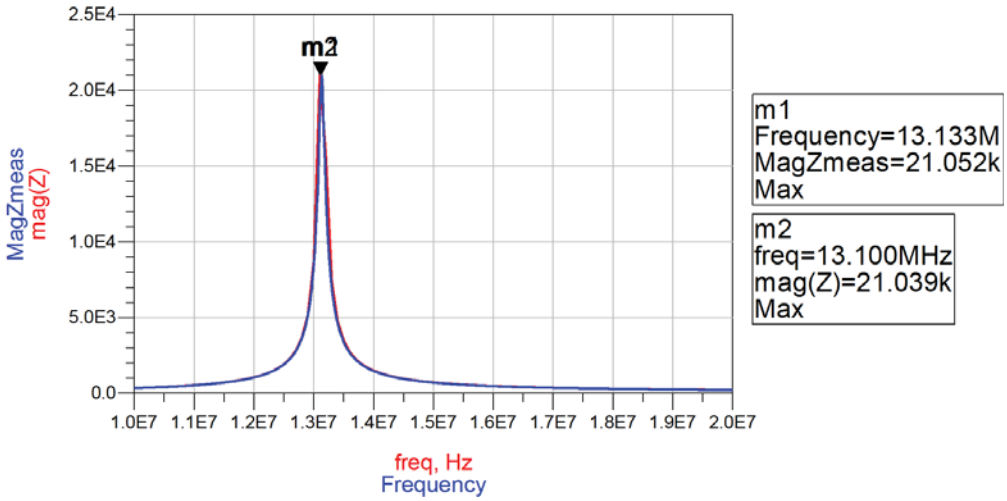

Figure 5.30: RefPICC antenna: Simulated curve fitted with measured curve

Afterwards, also the measured and simulated curves of RefPICC with load was investigated. For this analysis, the fine tuned values of the RefPICC antenna parameters were used. The measurement was performed again with passive components which should correspond the load (parallel circuit of R_p and C_p).

First load: • $R_p = 1\ \text{k}\Omega$ • $C_p = 27\ \text{pF}$

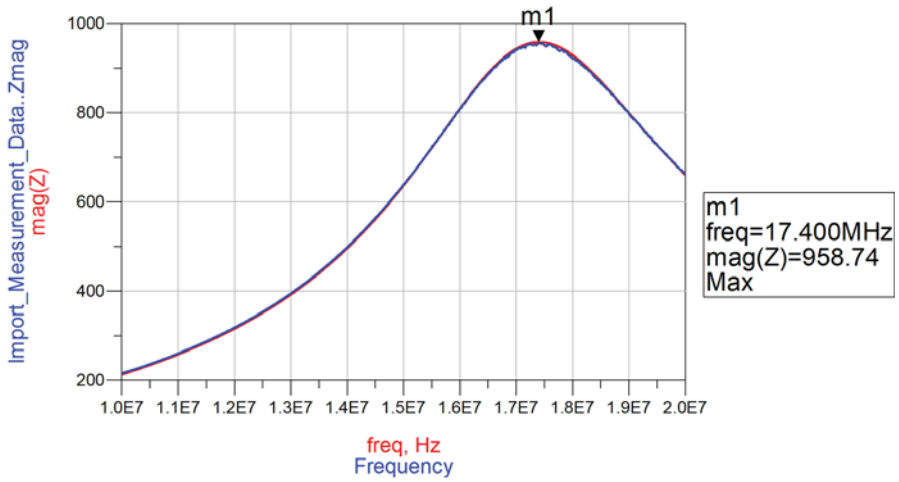

Figure 5.31: Matching through adjusting $R_p = 979\ \Omega$ and $C_p = 28.9\ \text{pF}$

Second load: • $R_p = 1\ \text{k}\Omega$ • $C_p = 90\ \text{pF}$

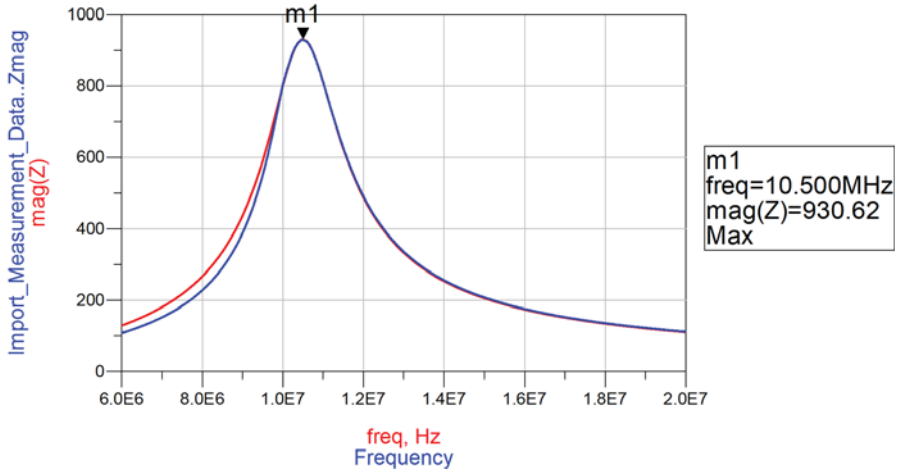

Figure 5.32: Almost matched through adjusting $R_p = 985\ \Omega$ and $C_p = 91.8\ \text{pF}$

Third load: • $R_p = 1\ \text{k}\Omega$ • $C_p = 100\ \text{pF}$

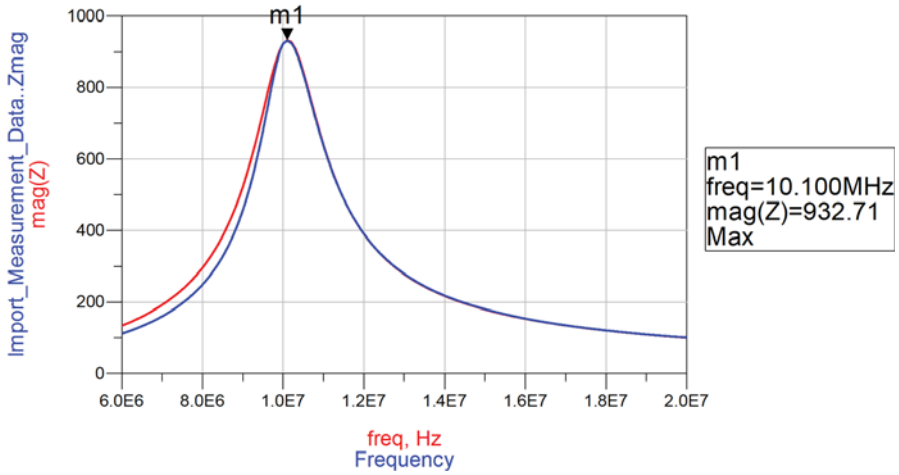

Figure 5.33: Almost matched through adjusting $R_p = 992\ \Omega$ and $C_p = 99.5\ \text{pF}$

The figure 5.31 illustrates that with a capacity of 27 pF a perfect curve fitting of both curves was possible. While examining the measured and simulated curves of RefPICC with capacities greater than 90 pF, it was noticeable that an accurate matching of both curves was not achievable. Only one half of the curves could be matched with fine tuning. In figures 5.32 and 5.33 it can be seen that only the right half of the curves were matched.

5.3.3.2 Curve fitting of EMV PCD at unloaded state

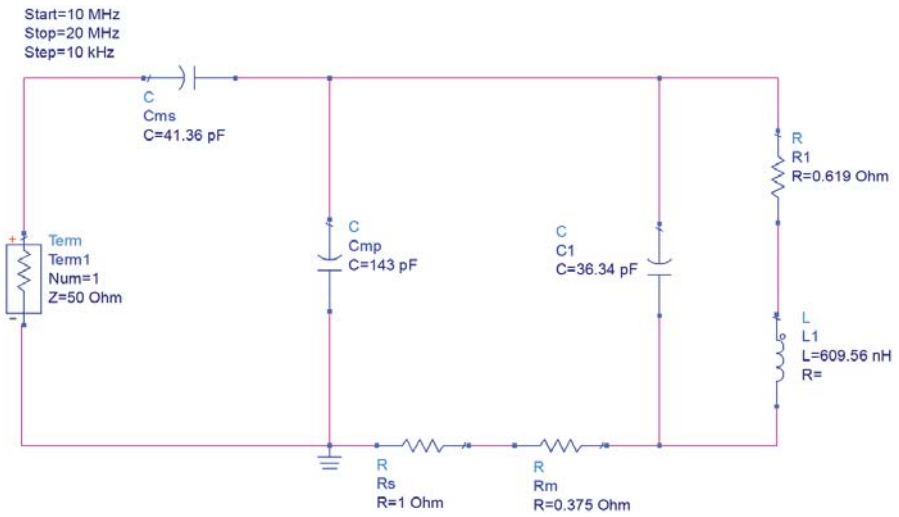

Figure 5.34: Simulation of the whole EMV PCD at unloaded state

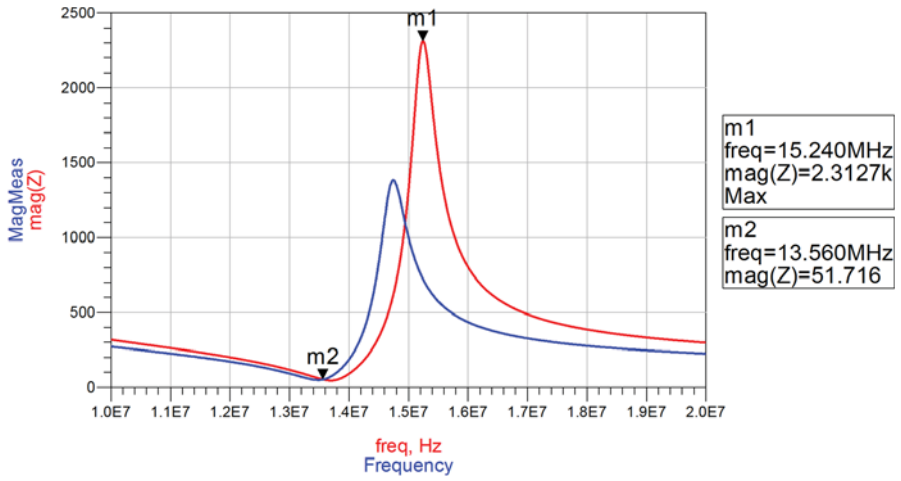

Figure 5.35: Impedance curve of measured and simulated EMV PCD at unloaded state

Figure 5.35 shows the outcome of the curve fitting of the EMV PCD. In this figure the significant mismatch between the simulation (red curve) and the measurement (blue curve) can be clearly seen. Hence the significant variation of the measured loading value and the simulated loading value with LMA-Tool at slot 0 can be argued. It can also be seen that the quality factor of the simulated curve is quite greater than the measured

curve. Both curves are only approximately matched at 13.56 MHz. It was impossible to match both curves through adjusting of approximately realistic EMV PCD parameter values. To reduce the high quality factor of the simulated curve, it has to be adjust to a higher resistance value for R_1, which would strongly deviate from the measured value. For further investigations both curves were matched at 13.56 MHz and an accurate matching of both curves with values which can also significantly differ from the realistic values.

1. Option: Simulation curve fitted at resonance frequency 13.56 MHz: For matching at resonance frequency only the matching capacities were tuned and the remaining EMV PCD parameters were unvaried. The following parameters were adjusted:

- $C_{ms,adjusted} = 40.1$ pF
- $C_{mp,adjusted} = 149.6$ pF

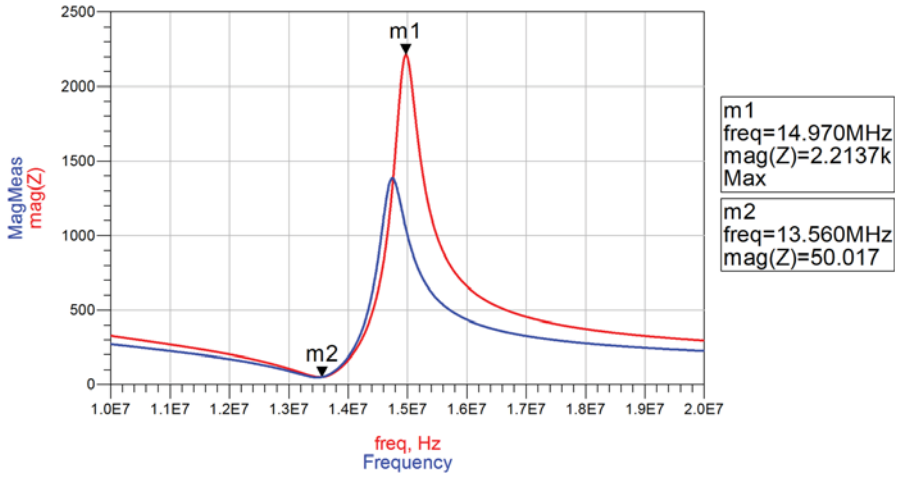

Figure 5.36: Curve fitting at resonance frequency 13.56 MHz

2. Option: Simulation curve completely fitted with the measurement curve: Except the resistances values of R_s and R_m, all the EMV PCD parameters were tuned. Thus, a complete matching of both curves was possible. It can be seen that especially the adjusted antenna parameters strongly vary from the measured values.

- $R_{1,adjusted} = 0.48312\ \Omega$
- $C_{1,adjusted} = 83.4$ pF
- $L_{1,adjusted} = 424.5568$ nH
- $C_{ms,adjusted} = 50.8552$ pF
- $C_{mp,adjusted} = 191.58$ pF

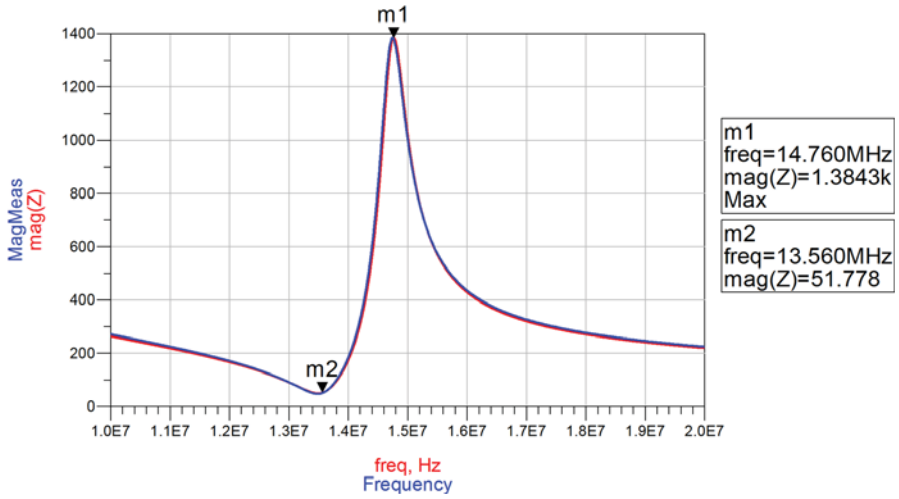

Figure 5.37: Accurate curve fitting of both curves

The new adjusted values of both options were implemented into the LMA-Tool in order to see if an improvement of the loading values, especially at slot 0, is achievable.

5.3.4 Results of LMA-Tool with new adjusted EMV PCD parameters

Measurement

$\hat{U}_{Rs,unloaded} = 0.712$V	
Loaded	
Slot number	$\hat{U}_{Rs}[V]$
Slot 0	0.621
Slot 1	0.668
Slot 2	0.68
Slot 3	0.687
Slot 4	0.693

(a)

1.Option		2.Option	
$\hat{U}_{Rs,unloaded} = 0.746$ V		$\hat{U}_{Rs,unloaded} = 0.748$ V	
Loaded		Loaded	
Slot number	$\hat{U}_{Rs}[V]$	Slot number	$\hat{U}_{Rs}[V]$
Slot 0	0.538	Slot 0	0.566
Slot 1	0.651	Slot 1	0.665
Slot 2	0.694	Slot 2	0.699
Slot 3	0.715	Slot 3	0.719
Slot 4	0.727	Slot 4	0.73

(b)

Table 5.9: Loading values of LMA-Tool with new adjusted EMV PCD parameters

Measurement

$\hat{U}_{Rs,unloaded} = 0.712$V	
Loaded	
Slot number	Loading[%]
Slot 0	12.78
Slot 1	6.18
Slot 2	4.49
Slot 3	3.51
Slot 4	2.67

(a)

1.Option		2.Option	
$\hat{U}_{Rs,unloaded} = 0.746$ V		$\hat{U}_{Rs,unloaded} = 0.748$ V	
Loaded		Loaded	
Slot number	Loading[%]	Slot number	Loading[%]
Slot 0	27.88	Slot 0	24.27
Slot 1	12.67	Slot 1	11.1
Slot 2	6.98	Slot 2	6.38
Slot 3	4.16	Slot 3	3.82
Slot 4	2.53	Slot 4	2.33

(b)

Table 5.10: Loading values of LMA-Tool with new adjusted EMV PCD parameters given as percentage

The table 5.9 b shows the outcomes of the simulated loading values, which were determined with the new tuned values of option 1 (matching at 13.56 MHz) and option 2 (complete matching of both curves). With the new adjustments of option 1 and option 2, the simulated value of $\hat{U}_{Rs,unloaded}$ is minimally increased and it differs from the measured value. The greatest deviation of the simulated loading value from the measured loading value happens again at slot 0. Even through complete matching through option 2, an improvement of the simulated loading value at slot 0 was not possible. The simulated loading values in the remaining slots match quite well with the measured values. Nevertheless, the table 5.10 shows that the percentage deviation, especially at slot 0 and slot 1 is still too great. Noticeable is that the simulated values differ from measured values in the second or third position after the decimal point and the percentage deviation is still to high. Thus, it can be argued that the accuracy of simulated values is very essential in order to reduce the percentage deviation of measurement and simulation.

Chapter 6: Conclusion

Nowadays the RFID technology is used in different areas of our daily life and depending on its use it has to fulfill various requirements. In order to guarantee impeccable function of the chip cards, they have to be thoroughly tested with the respective test set-up. The two commonly applied test methods are the ISO set-up and the EMVCo set-up. Whereas the EMVCo set-up is only used for payment applications and the ISO set-up is utilized for almost all remaining applications. This work deals with an approach with which EMVCo related values are determined out of ISO measurement. Thus, it is attempted to form out of both measurements only one measurement as the EMVCo measurement is very laborious and time-consuming.

6.1 Measurement and Simulation Results

Primarily, a thoroughly reading up on the RFID-basics was essential in order to get a fundamental knowledge and a better understanding of the RFID system. Then, first measurements with the two prevalent test set-ups were done. Thanks to this the main differences in structure and measuring process of both test set-ups could be clearer understand. A simple field strength sweep measurement of a chip with the ISO-tower was done whereby a data acquisition tool of Infineon saves the two voltages (u_{cal} and u_d) of the ISO-tower for each field strength point. Through these voltages the LMA-Tool determines the chip parameters (R_p and C_p) for each field strength point. Thus it is possible to generate a LUT, which shows the corresponding chip parameters for each field strength point. A LUT was important for the approximate iterative determination of the chip parameters ($R_{p,EMV}$ and $C_{p,EMV}$), which the chip would adjust in the different slots of the operating volume of the EMVCo set-up. Subsequently, the simplified equivalent circuit of the EMVCo set-up was implemented in the LMA-Tool. For the iterative determination a reference value was relevant, which increases monotonically

within the adjusted field strength range. The determination of real power P_{real} of the chip had shown that P_{real} has the required property of the reference value. So far, the gradual determination of $R_{p,EMV}$ and $C_{p,EMV}$ out of the ISO measurement works for the RX-mode for the field strength range between 1 A/m and 10 A/m with a step of 0.2 A/m and for a chip resonance frequency of 17 MHz. After the approximate iterative determination of $R_{p,EMV}$ and $C_{p,EMV}$ for each slot with LMA-Tool, only then it was possible to calculate the corresponding loading values. Next, the measured loading values were compared with the simulated loading values. Hence it was noticed, that the loading values at slot 0 strongly deviated from one another. The simulated loading values at the remaining slots matched quite well with the measured values. They only differ from one another in the second or third position after the decimal point. In order to improve the simulated loading value at slot 0, the EMV PCD antenna parameters, the coupling coefficients for each slot and the RefPICC antenna parameters were measured again. These measurements have shown that the new measured parameters do not strongly differ from the previous measured parameters. Additionally, the measured EMV antenna and RefPICC antenna parameters were examined also through curve fitting, where the measured and the simulated impedance curves of both antennas were compared. The result of the curve fittings showed that the measured and the simulated curves quite accurately match with each other. Thus it can be argued, that the measured antenna parameters were quite well determined. Afterwards, the RefPICC with load (parallel circuit of passive components) and the whole EMV PCD was investigated through curve fitting in order to examine how strongly the measurement and the simulation results differ from one another. The measured and the simulated impedance curves of the RefPICC with load (R_p and C_p) differ only minimal from one another, but it was noticed that with a load capacitance greater than 90 pF, only one half of the simulated curve could be matched with the measured curve. The curve fitting outcome of the whole EMV PCD clearly illustrated that the measured and the simulated impedance curves significantly deviate from each other. Hence, it can be argued, that the possible reason for a mismatch at slot 0 is the significant deviation of measurement result from the simulation result. An accurate matching of both curves with realistic values, which do not strongly differ from the measured values, was impossible. For further examination of loading values, the simulated curve was matched at 13.56 MHz only with matching capacities with the measured curve and also the simulated curve was almost accurately matched with the measured curve by varying the EMV PCD parameters,

which significantly differed from the realistic values. It was noticeable, that also with the new adjusted EMV PCD parameters of both options, the loading value determined through the LMA-Tool significantly differs from the measured loading value at slot 0. The loading values for the remaining slots were again well matched, but the percentage deviation of simulated values from the measured values for slot 0 and slot 1 is still too high.

6.2 Outlook

To sum up, this master's thesis has attempted to deliver EMVCo related values through an iterative determination with chip parameters out of ISO measurement. In general, it can be said, that the iterative determination of EMVCo pertinent values is possible, but it has to be examined for also different field strength range, different steps and for different chip resonance frequencies. The curve fitting of EMV PCD has showed that the measurement significantly mismatches with the simulation. Thus, the assumed equivalent circuit of the EMV PCD has to be improved or extended in order to get accurate simulated loading values. Additionally, the accuracy of the parameter determination is also important, especially the coupling coefficients, in order to reduce the deviation between simulated and measured loading values.

Bibliography

[1] Egger, C.: Reference PICC for Extended Modulation and LMA Measurement Principles. Master's thesis, 2013.

[2] EMVCo: EMVCo Type Approval Contactless Terminal Level 1. Techn. Rep. Version 2.1a, 2011. PCD Analogue Test Bench and Test Case Requirements.

[3] EMVCo: A Guide to EMV, 2011. http://paysmart.com.br/wp-content/uploads/2013/03/EMVCo-A-Guide-to-EMV.pdf.

[4] EMVCo: EMV Specifications for Payment Systems - Book D. Techn. Rep. Version 2.4, 2014. EMV Contactless Communication Protocol Specification.

[5] Finkenzeller, K.: RFID-Handbuch - 4.Auflage. Carl Hanser Verlag, 2006.

[6] Gebhart, M.: Vorlesung RFID Systems, 2011. http://rfid-systems.at/08_Testverfahren_2011.pdf.

[7] Gebhart, M.: Vorlesung RFID Systems, 2011. http://rfid-systems.at/06_Kartenherstellung_2011.pdf.

[8] Gebhart, M., W. Eber, W. Winkler, D. Kovac and H. Krepelka: From Power to Performance in 13.56 MHz Contactless Credit Card Technology. Techn. Rep., 2008. http://rfid-systems.at/002.pdf.

[9] Hölzl, J.: Extended Card Modulation - Test Methods. Master's thesis, 2011.

[10] Infineon Technologies AG: Transport Ticketing: Driving multi-application and transport ticketing on open standards. http://www.infineon.com/dgdl/Transport+%26+Ticketing.pdf?fileId=db3a30432a7fedfc012aa3493839331a.

[11] ISO/IEC: ISO/IEC 14443-2, Identification cards: Contactless integrated circuit cards - Proximity cards. Techn. Rep. Part 2: Radio frequency power and signal interface, Committee identification: ISO/IEC JTC1/SC17/WG8, 2013.

[12] ISO/IEC: ISO/IEC 10373, Identification cards - Test methods. Techn. Rep. Part 6: Proximity cards, Committee identification: ISO/IEC JTC1/SC17/WG8, 2014-07-14.

[13] Meier, T., G. Egger and M. Gebhart: Nachrichtentechnik, Labor: RFID, 2007. Institut für Kommunikationsnetze und Satellitenkommunikation der Technischen Universität Graz.

[14] Paill, K.: Physik, Band 2. E. Dorner, 2001.

[15] Rampetzreiter, S.: Very High Bit Rate Communication Channel Modeling on Inductively Coupled, Passive RFID Systems. Master's thesis, 2009.

[16] Renhart, W.: Ergänzende Unterlagen zur Vorlesung Grundlagen der Elektrotechnik (ET) - Teil 2, 2011. http://igte.cats-host.com/cms/images/stories/lehrveranstaltungen/437_209/437_209_get_et.pdf.

[17] Zastrow, D.: Elektrotechnik: Lehr- und Arbeitsbuch. Vieweg Verlag, 1993.